The Adriatic Sea General Circulation. Part I: Air–Sea Interactions and Water Mass Structure

A. ARTEGIANI,* D. BREGANT,+ E. PASCHINI,* N. PINARDI,# F. RAICICH,+ AND A. RUSSO*

* *Istituto di Richerche sulla Pesca Marittima, CNR, Ancona, Italy*
+ *Istituto Talassografico di Trieste, CNR, Trieste, Italy*
# *Istituto per lo Studio delle Metodologie Geofisiche Ambientali, CNR, Bologna, Italy*

(Manuscript received 3 March 1995, in final form 5 March 1996)

ABSTRACT

A comprehensive historical hydrographic dataset for the overall Adriatic Sea basin is analyzed in order to define the open ocean seasonal climatology of the basin. The authors also define the regional climatological seasons computing the average monthly values of heat fluxes and heat storage from a variety of atmospheric datasets. The long term mean surface heat balance corresponds to a heat loss of 19–22 W m^{-2}. Thus, in steady state, the Adriatic should import about the same amount of heat from the northern Ionian Sea through the Otranto Channel. The freshwater balance of the Adriatic Sea is defined by computing the average monthly values of evaporation, precipitation, and river runoff, obtaining an annual average gain of 1.14 m. The distribution of heat marks the difference between eastern and western Adriatic areas, showing the winter heat losses in different parts of the basin.

Climatological water masses are defined for three regions of the Adriatic: (i) the northern Adriatic where seasonal variations in temperature penetrate to the bottom; deep water (NAdDW) with $\sigma_t > 29.2$ kg m^{-3} is produced and salinity is greatly affected by river discharges; (ii) the middle Adriatic where a pool of modified NAdDW is stored during the summer season after being renewed in winter and modified Levantine Intermediate Water (MLIW) intrudes from the southern regions between spring and autumn; and (iii) the southern Adriatic where homogeneous water properties are found below 150 m (the local maximum depth of the seasonal thermocline) and a different deep water mass (SAdDW) is found with $\sigma_t > 29.1$ kg m^{-3}, $T \approx 13.5$°C, and $S \approx 38.6$ psu. Due to river runoff waters, the surface layers of all three regions are freshened during the spring–summer seasons. The vertical distributions of dissolved oxygen vary quantitatively in the three regions showing a spring–summer subsurface maximum due to the balance between phytoplankton growth in the euphotic zone and low vertical mixing in the water column. This behavior can be reconciled with open ocean conditions except for the northernmost part of the Adriatic where well-mixed oxygen conditions prevail throughout the year.

Large interannual anomalies of both temperature and salinity are found at the geographical center of the basin in surface and deep waters (100 m).

1. Introduction

The Adriatic Sea (Fig. 1) is an elongated basin, with its major axis in the northwest–southeast direction, located in the central Mediterranean, between the Italian peninsula and the Balkans. Its northern section is very shallow and gently sloping, with an average bottom depth of about 35 m. The middle Adriatic is 140 m deep on average, with the two Pomo Depressions reaching 260 m. The southern section is characterized by a wide depression more than 1200 m deep. The water exchange with the Mediterranean Sea takes place through the Otranto Channel, whose sill is 800 m deep.

The eastern coast is generally high and rocky, whereas the western coast is low and mostly sandy. A large number of rivers discharge into the basin, with significant influence on the circulation, particularly relevant being the Po River in the northern basin, and the ensemble of the Albanian rivers in the southern basin.

Studies of the Adriatic Sea started in the early eighteenth century, although a few observations are reported earlier, and essentially concerned the coastal biological phenomenology, whereas open-sea observations began in the nineteenth century. Several aspects of such research have been reported by many authors in the past, so that more details can be found in their papers (D'Ancona and Picotti 1958; Pigorini 1968; Trotti 1969; Buljan and Zore-Armanda 1976; Zavodnik 1983; Artegiani et al. 1993).

Among those activities, the most significant contribution to the knowledge of the physical characteristics of the basin was provided by the series of seasonal cruises made by the Permanent Italian–Austrian Commission in the years 1911–14 (R. Comitato Talasso-

Corresponding author address: Dr. Fabio Raicich, Istituto Sperimentale Talassografico, CNR,Viale Romolo Gessi 2, I-34123 Trieste, Italy.
E-mail: raicich@ts.cnr.it

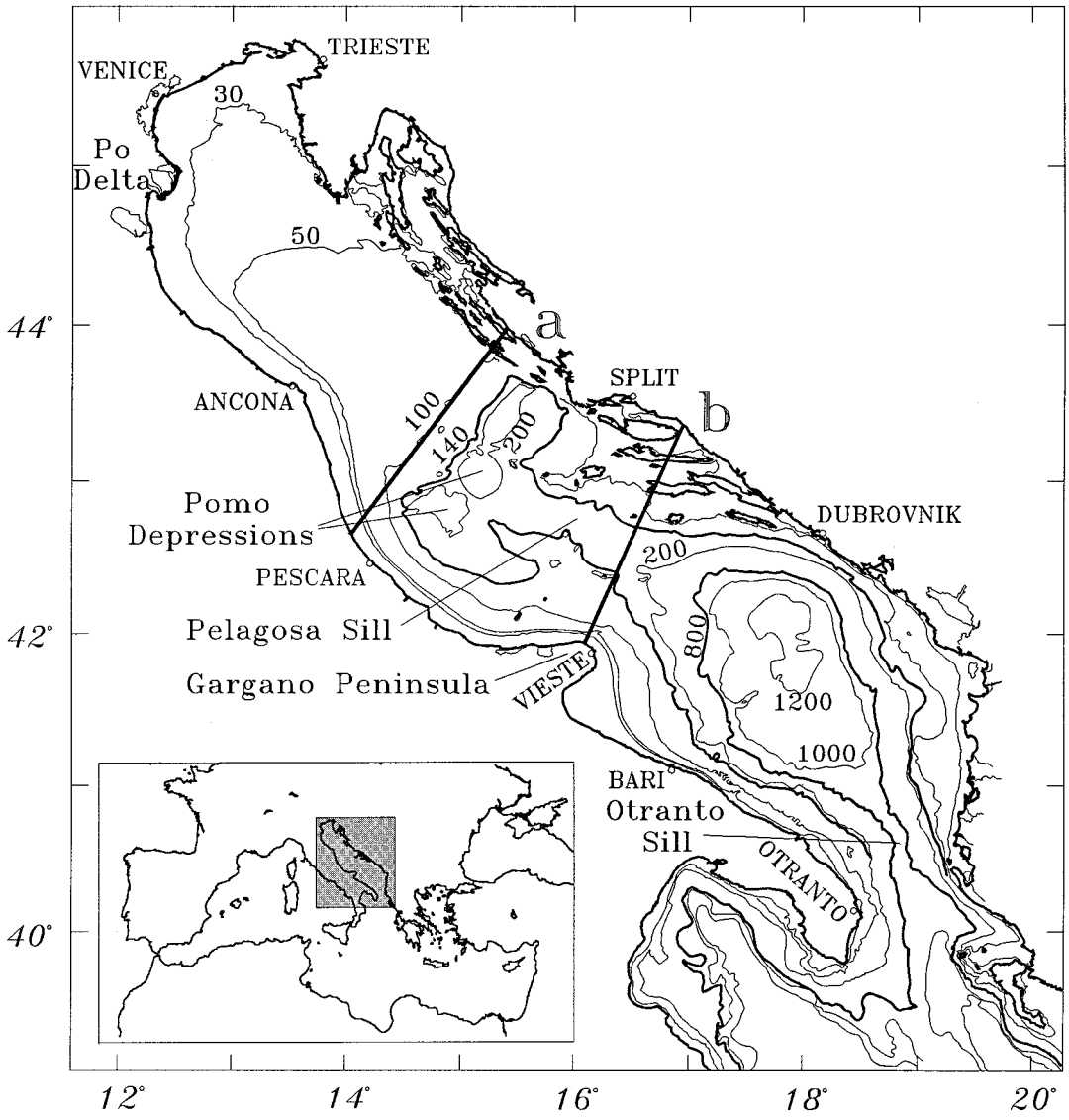

FIG. 1. Adriatic Sea coastline and topography. Lines *a* and *b* define the northern, middle, and southern subbasins.

grafico 1912, 1913, 1914; Brückner 1912, 1913, 1915). The results from these early cruises defined the basic knowledge of the basin phenomenology and the starting point for subsequent investigations up to the beginning of the 1980s.

Between the two world wars relevant contributions did not occur, although both Italian and Yugoslav researchers continued the observations and studies. Since World War II there has been an increasing amount of research, starting with Yugoslav surveys in 1947 (Buljan and Marinković 1956) and the Italian cruise of 1955 (D'Ancona and Picotti 1958). The research was stimulated also by environmental problems induced by the occurrence of anomalous phenomena, like strong storm surges, intense algal blooms, and the presence of gelatinous masses.

The large amount of data collected enabled the researchers to outline, even if not always in a satisfactory manner, some basic processes, such as the dense water formation and the role of river discharges. Most of the analysis has been performed in the northern basin (Franco 1970, 1972, 1982), so that its phenomenology is relatively well known, compared to that of the middle and, especially, the southern basin (Artegiani et al. 1993).

Here we analyze the hydrochemical dataset composed of almost all data collected from the beginning of the century to the early 1980s for the entire Adriatic Sea. This allows us to infer the structure of the general circulation of the overall basin. In Part I of the paper we analyze the air–sea interaction budgets and the water mass structure of the basin. In Part II (Artegiani et al. 1997) we describe the horizontal circulation features. In section 2 of Part I we define the air–sea heat and mo-

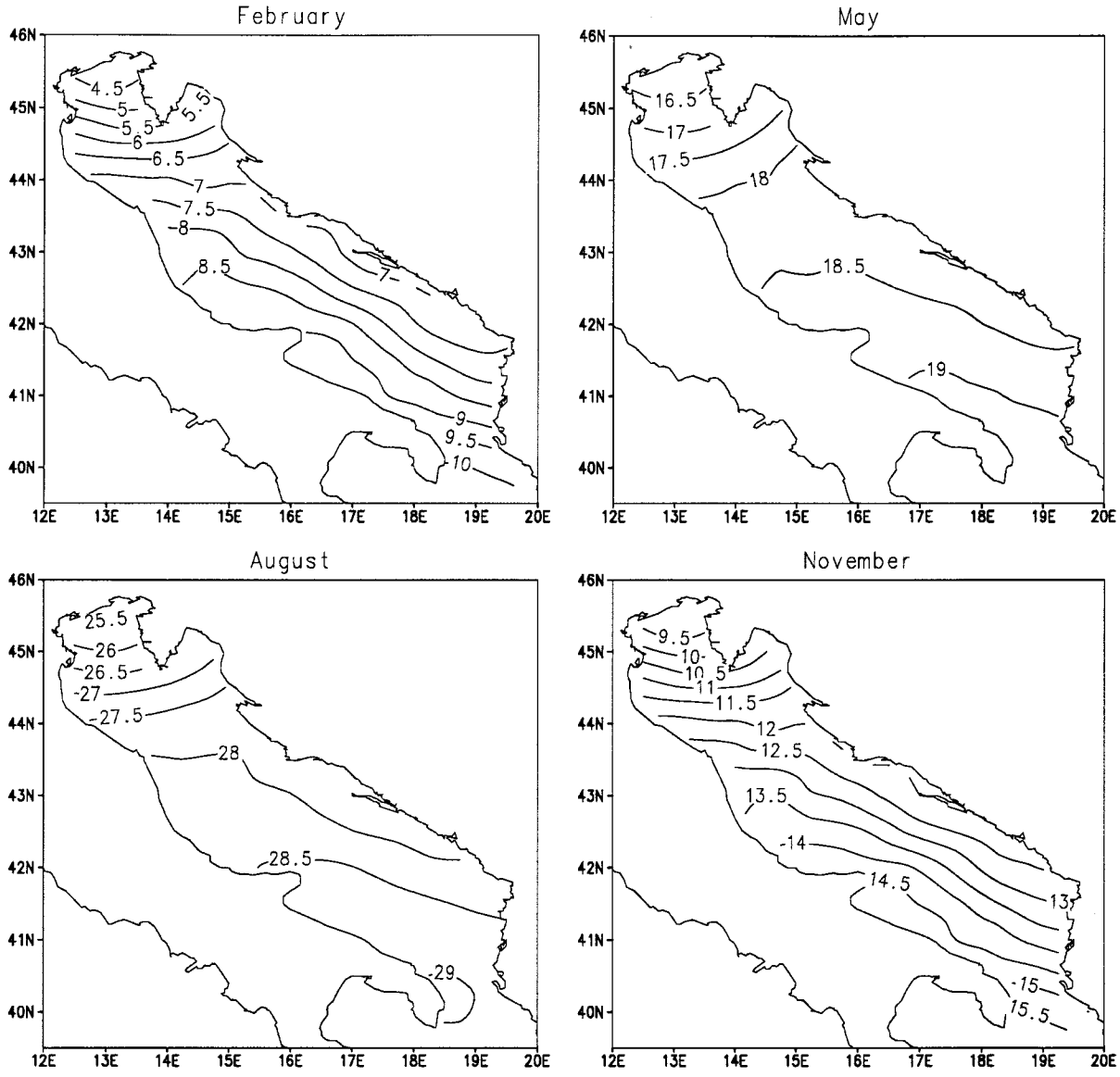

FIG. 2a. Maps of February, May, August, and November average air temperature (°C) from the NMC dataset at 1000 hPa.

mentum fluxes for the overall region, classify the seasons on the basis of the Adriatic overall heat storage, and determine the fresh water balance. The dataset is described in section 3, and we classify the water masses and the oxygen distribution in section 4. In section 5 we describe the seasonal variations of water masses along some selected vertical sections. Interannual variability is analyzed at the available stations in section 6. Finally, conclusions are presented in section 7.

2. Atmospheric conditions, season definition, heat, and freshwater budgets

Here we give a climatological description of the atmospheric conditions over the basin, and their effect in terms of heat exchange and storage. One of the datasets used was obtained from the National Meteorological Center (renamed the National Centers for Environmental Prediction). It consists of 12-h operational analysis fields at 1000 hPa, with $1° \times 1°$ spatial resolution, for air temperature, relative humidity, and wind speed for the period January 1980–December 1988. The original dataset has been averaged to produce climatological monthly mean values of the variables, shown in Figs. 2a–c for the months of February, May, August, and November, which may be regarded as representative of each season.

Air temperature (Fig. 2a) exhibits seasonal fluctuations of about 20°C over the entire basin. A longitudinal gradient prevails in the northernmost section, whereas a transverse gradient is dominant in the middle and southern Adriatic. The north–south temperature differ-

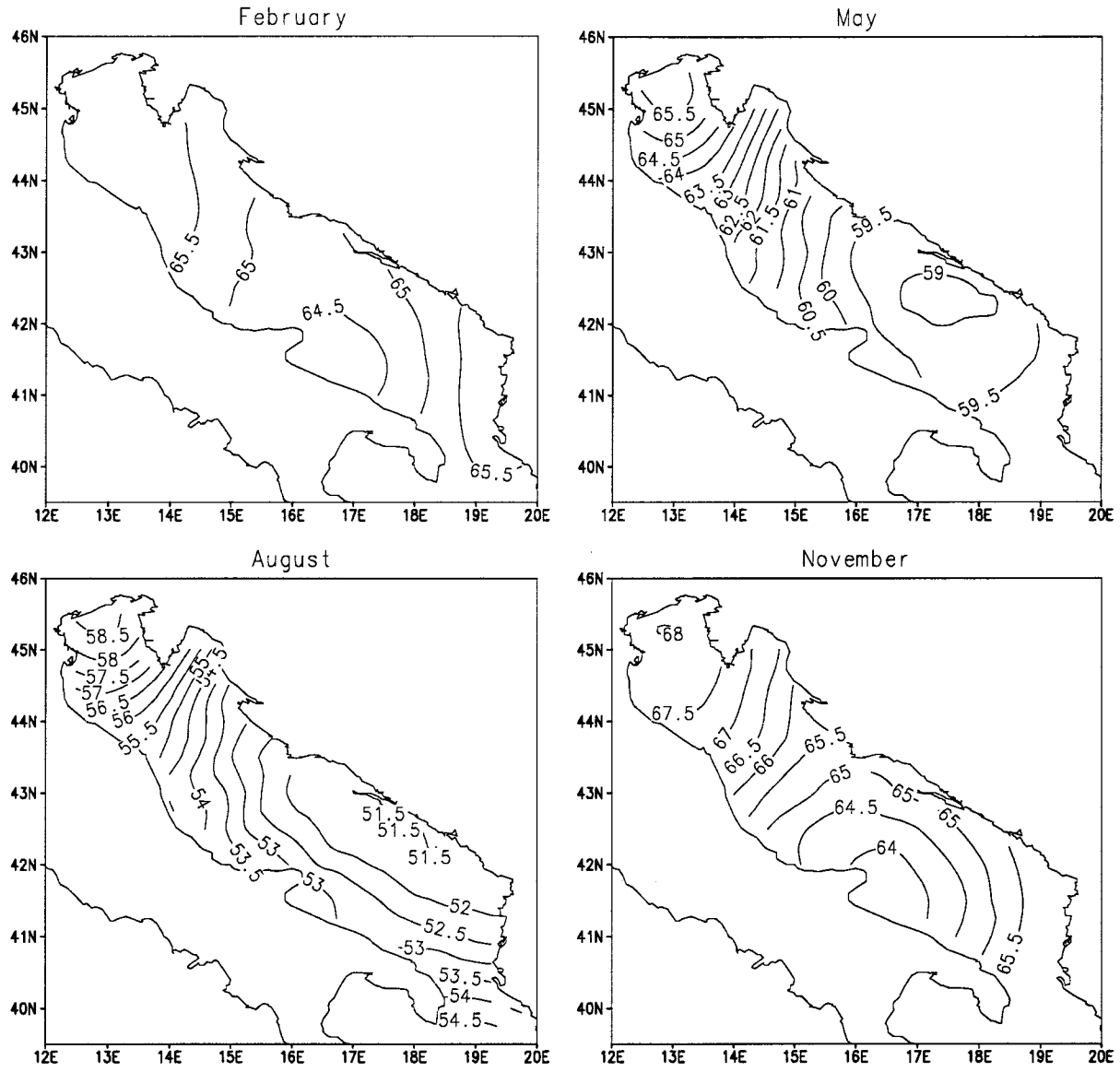

FIG. 2b. Maps of February, May, August, and November average relative humidity (%) from the NMC dataset at 1000 hPa.

ence ranges from about 3.5°C in May to about 7°C in November.

Relative humidity (Fig. 2b) is generally higher in the northern section and in the colder seasons, mainly as a consequence of lower air temperature. The winter field is relatively homogeneous, whereas a significant longitudinal gradient exists in the northern section in spring and summer. A relative humidity minimum is present in all seasons in the southern section.

The main characteristic of NMC wind data (Fig. 2c) is a prevailing westerly component in all seasons; however, the two other datasets examined, Hellerman and Rosenstein (1983) and May (1982), exhibit a dominant easterly component, at least over the northern and middle Adriatic, in agreement with the frequent observations of northeasterly and southeasterly winds made at most of the coastal meteorological stations. In Fig. 2d February and November maps of Hellerman and Rosenstein's and May's data are shown for comparison. We believe that the climatological NMC wind field is too zonal over this region and shows smaller intermonthly variations than the other climatological datasets; however, it is a dataset that provides consistent wind and temperature fields over the area.

The adopted monthly mean cloudiness fields come from the Comprehensive Ocean Atmosphere Data Set (COADS). Cloudiness varies approximately between two-tenths in July and six-tenths in January and February and is rather uniformly distributed over the whole

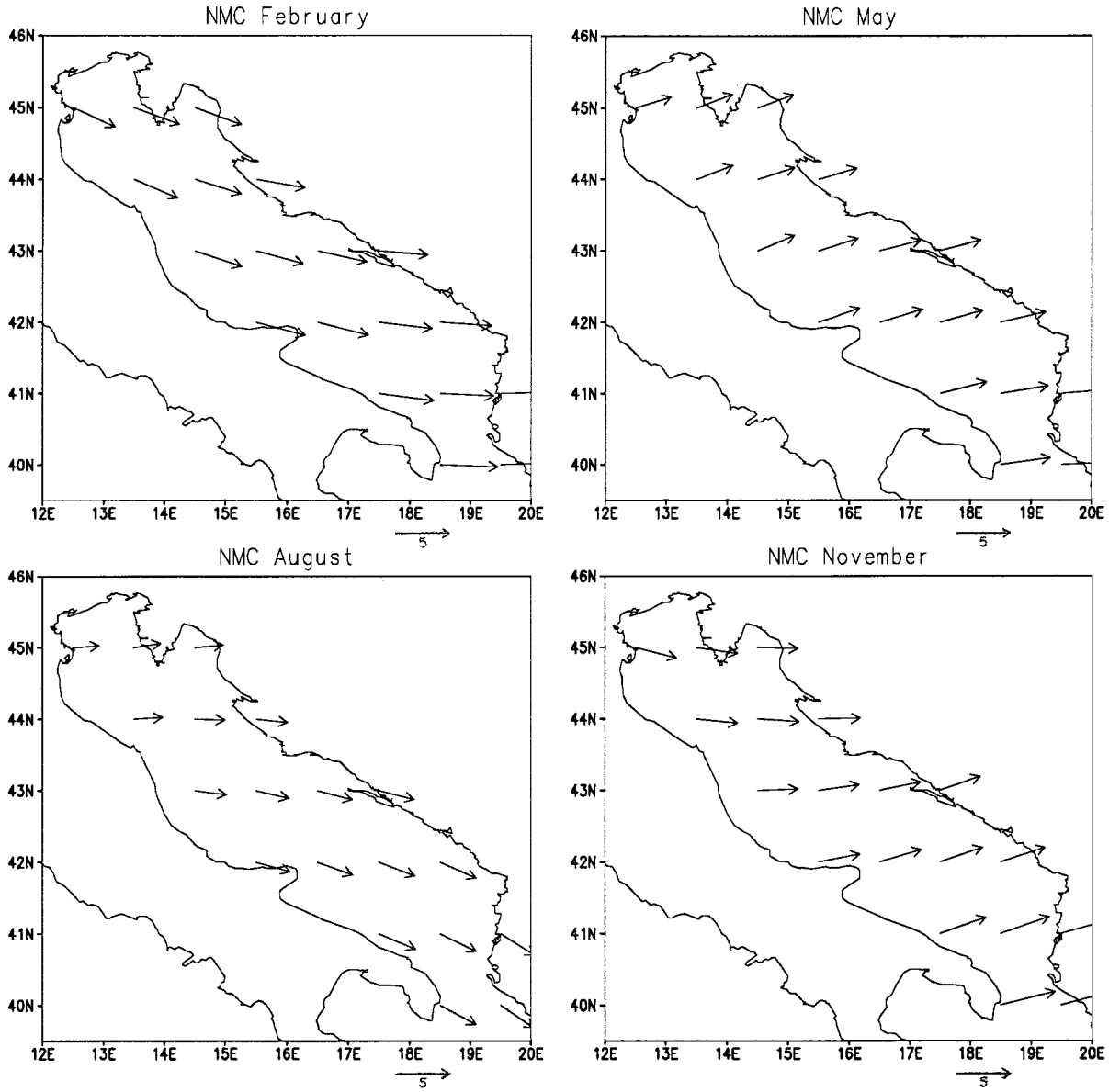

FIG. 2c. Maps of February, May, August, and November average wind speed (m s^{-1}) from the NMC dataset at 1000 hPa.

basin, the standard deviation associated with the spatial mean being about 10%.

Figure 2e shows the average fields of total heat flux resulting from the May dataset (May 1986) for selected months representing each season, namely, February, May, August, and November. We decided to display the May dataset since it covers the entire basin, while the COADS cloudiness dataset does not include some coastal areas. A strong cooling occurs everywhere in November, particularly in the northern region, while in February the maximum heat loss is found in the middle Adriatic close to the western coast. In May a transverse gradient is present, while in August a longitudinal gradient occurs in the northern and middle regions. The maximum heat losses along the Italian coastline during winter–spring months may support the conclusion that the western Adriatic coastal areas are dominated by downwelling processes. This conclusion is also supported by the presence of downwelling-favorable northerly winds in winter and spring.

We have computed the climatological monthly heat budget at the sea surface by means of the bulk formulas selected by Castellari et al. (1997, manuscript submitted to *J. Mar. Res.*, hereafter referred to as CPL97) (see the appendix), using the atmospheric data described above. The monthly mean sea surface temperature fields are obtained from our hydrological dataset and will be discussed later. To verify that the NMC wind pattern did not affect our heat budget computations, we used all three climatological wind datasets described above

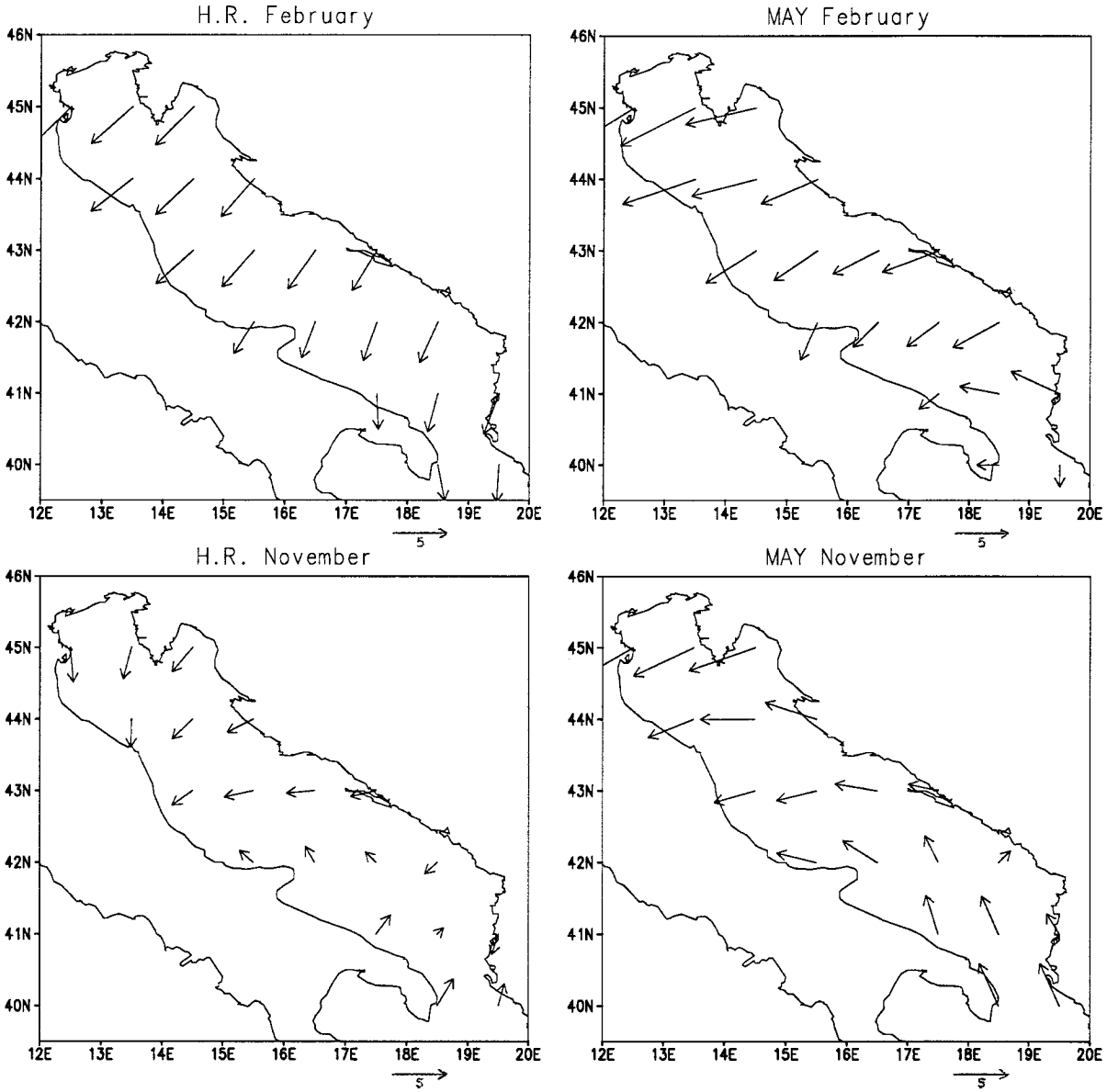

FIG. 2d. Comparison between wind speeds (m s^{-1}) from Hellerman and Rosenstein (HR, left) and May (right).

(NMC, Hellerman and Rosenstein, and May). As we can see in Fig. 3, the differences in wind direction did not appreciably change the heat budget calculations.

Table 1 summarizes each heat budget component computed by means of the NMC air temperature, relative humidity, and wind data. We see that latent and longwave radiation heat fluxes dominate the balance together with the shortwave incoming solar radiation. The annual average of the NMC heat budget is about -19 ± 10 W m^{-2}. For a comparison, we have also computed the same quantities from the May dataset (Table 2). The annual average of May total heat flux is -22 W m^{-2} (no statistical error has been reported), which is compatible with the value obtained from the fluxes summarized in Table 1. Significant differences can be seen in the comparison of individual monthly values of the flux components, such as the summer values of the latent heat flux. This can be partly explained as follows: (i) the datasets cover different periods, since May used observations from 1945 to 1984, while we used atmospheric data for the period 1980–88 and sea surface temperatures for the periods 1911–14 and 1947–83; (ii) May first computed the fluxes from each individual observation and subsequently calculated the spatial and time averages, while the scarcity of available observations forced us to use the space and time averaged values of the observations directly in the bulk formulas. Furthermore, we decided to use different bulk formulas

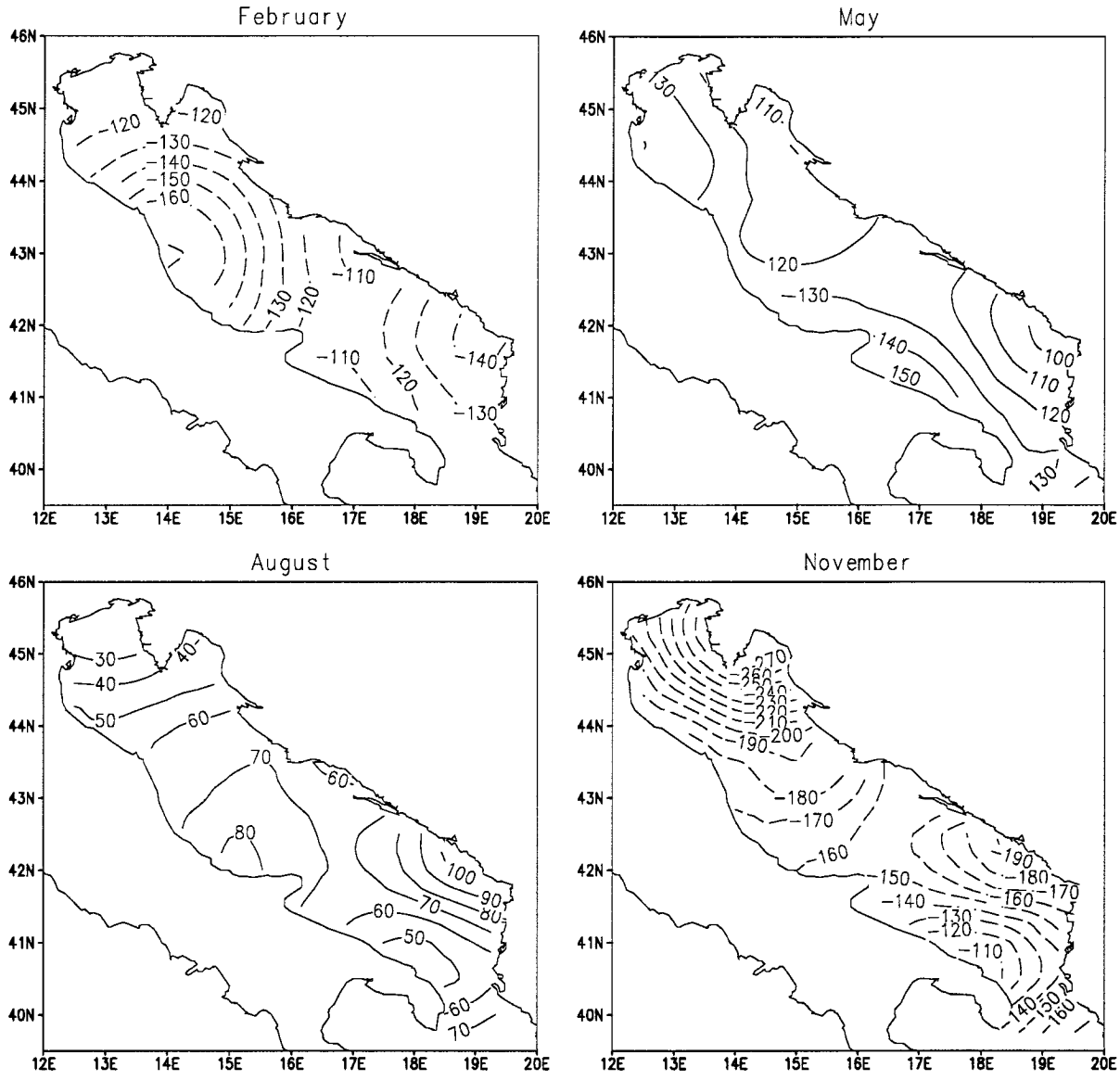

FIG. 2e. Maps of February, May, August, and November average surface total heat flux (W m $^{-2}$) from May (1986). The contour interval is 10 W m^{-2} and the dashed lines indicate negative values.

than May and this may affect the estimates of individual terms (CPL97).

The negative annual average of the surface heat flux implies that in steady-state conditions the Adriatic imports heat from the Mediterranean. This is expected due to the deep-water formation processes occurring in the winter and the known outflow–inflow system at Otranto (Ferentinos and Kastanos 1988; Michelato and Kovačević 1991). Warmer surface waters enter at Otranto, while at depth there is a net outflow of cold deep waters. Due to data paucity, the evaluation of heat transport from the hydrographic data would not be reliable and we leave this question for future studies.

In order to arrange our hydrographic dataset on a seasonal basis, we have defined the ''ocean'' seasons according to Anati (1977). His method is based on the computation of the climatological heat storage in the top layer, where the atmospheric influence mostly occurs. The definition of relative heat storage (HS) is taken from Hecht et al. (1985):

$$\mathrm{HS} = \frac{D}{\mathrm{H}} \int_{-\mathrm{H}}^{0} c_p \rho (T - T_0)\, dz \qquad \text{if } \mathrm{H} < D$$

$$\mathrm{HS} = \int_{-D}^{0} c_p \rho (T - T_0)\, dz \qquad \text{if } \mathrm{H} \geq D, \quad (1)$$

where H is the actual water column depth, D is the

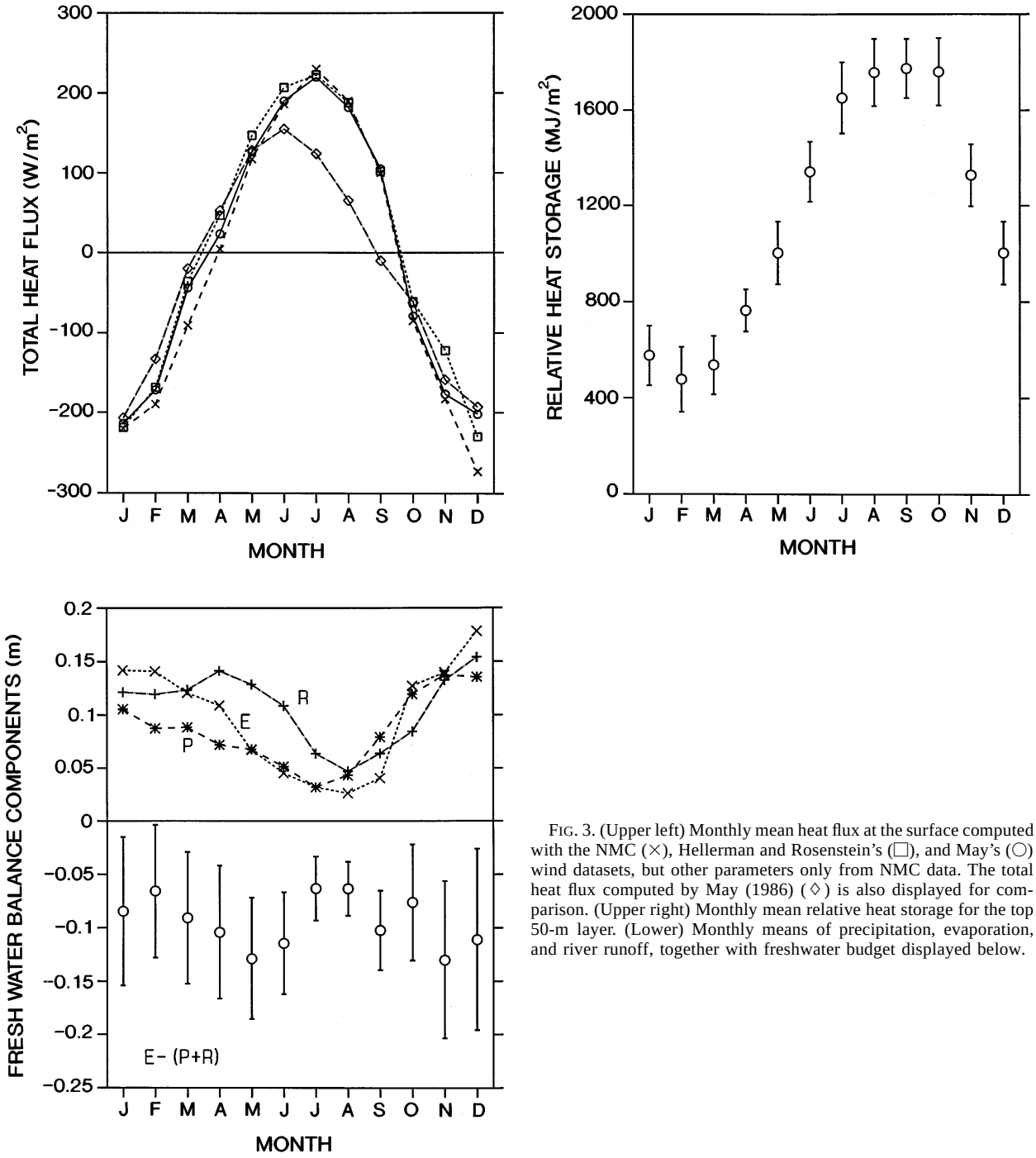

FIG. 3. (Upper left) Monthly mean heat flux at the surface computed with the NMC (×), Hellerman and Rosenstein's (□), and May's (○) wind datasets, but other parameters only from NMC data. The total heat flux computed by May (1986) (◇) is also displayed for comparison. (Upper right) Monthly mean relative heat storage for the top 50-m layer. (Lower) Monthly means of precipitation, evaporation, and river runoff, together with freshwater budget displayed below.

maximum water depth considered, c_p the specific heat at constant pressure, ρ the in situ density, T the water temperature, and T_0 an arbitrary reference temperature. In our computations $D = 50$ m, c_p has been computed according to Fofonoff and Millard (1983), ρ and T have been derived from our dataset, and $T_0 = 10$°C. For the purpose of seasonal definition, we are not interested in the actual heat storage values, but rather in its annual cycle, which turns out to be almost insensitive to D greater than 50 m and less than 150 m. The relative heat storage is shown in Fig. 3. Two extreme seasons can be clearly distinguished, namely, winter from January to April, and summer from July to October. We can also define the two transition seasons: spring, consisting of May and June, and autumn, consisting of November and December.

TABLE 1. Monthly surface heat flux components from NMC air temperature, relative humidity, and wind data, COADS cloud data and sea surface temperature of our dataset: Q_S is the incident solar radiation flux, Q_B the backward radiation flux, Q_H the sensible heat flux, Q_E the latent heat flux, and Q the total heat flux (see the appendix). All units are in W m^{-2}; the annual average is -19 ± 10 W m^{-2}.

Month	Q_S	Q_B	Q_H	Q_E	Q
Jan	51	-87 ± 2	-50 ± 2	-135 ± 5	-221 ± 7
Feb	81	-88 ± 2	-51 ± 2	-134 ± 5	-192 ± 7
Mar	131	-80 ± 2	-28 ± 3	-115 ± 6	-92 ± 7
Apr	198	-80 ± 3	-12 ± 3	-103 ± 7	3 ± 9
May	238	-63 ± 3	5 ± 2	-64 ± 11	116 ± 12
Jun	282	-59 ± 5	6 ± 1	-43 ± 11	186 ± 12
Jul	302	-50 ± 6	7 ± 1	-30 ± 8	229 ± 11
Aug	256	-49 ± 6	5 ± 1	-25 ± 7	188 ± 9
Sep	187	-56 ± 5	6 ± 1	-38 ± 11	99 ± 13
Oct	119	-76 ± 4	-10 ± 1	-120 ± 13	-87 ± 15
Nov	64	-84 ± 3	-32 ± 3	-133 ± 7	-185 ± 9
Dec	46	-93 ± 2	-59 ± 3	-170 ± 6	-275 ± 8

TABLE 2. May's monthly surface heat flux components: Q_S is the incident solar radiation flux, Q_B the backward radiation flux, Q_H the sensible heat flux, Q_E the latent heat flux, and Q the total heat flux (see the appendix). All units are in W m^{-2}; the annual average is -22 W m^{-2}

Month	Q_S	Q_B	Q_H	Q_E	Q
Jan	66	-76	-48	-148	-207
Feb	99	-73	-36	-123	-133
Mar	153	-69	-16	-88	-20
Apr	201	-67	-9	-74	52
May	251	-61	-2	-61	128
Jun	283	-59	0	-69	155
Jul	296	-64	-2	-105	124
Aug	254	-66	-6	-117	65
Sep	196	-69	-12	-125	-10
Oct	133	-70	-13	-112	-62
Nov	77	-71	-30	-135	-159
Dec	55	-70	-38	-141	-193

The relationship between the heat storage and total surface heat flux Q can be written as follows:

$$(\mathrm{HS})_t = Q - \mathbf{v} \cdot \boldsymbol{\nabla}(\mathrm{HS}) - K_H \nabla^2(\mathrm{HS}) + w\,\mathrm{HS}\big|_{z=-D} - K_V c_p \rho T_z\big|_{z=-D}. \quad (2)$$

The advective term in the right-hand side is dominated by its horizontal components $\mathbf{v}$, since the vertical velocity w is much smaller than the horizontal velocity and since its influence has been reduced due to the vertical integration. If we now integrate horizontally and make these approximations, Eq. (2) becomes

$$\iint_A (\mathrm{HS})_t\, dA = \iint_A Q\, dA - \int_O \mathbf{v}\cdot\mathbf{n}\mathrm{HS}\, dl + K_H \int_O \boldsymbol{\nabla}(\mathrm{HS})\cdot\mathbf{n}\, dl, \quad (3)$$

where A is the surface of the Adriatic basin and O its boundary across the Otranto Channel. The upward or downward heat flux at the base of the seasonal thermocline layer is considered to be negligible when the horizontal average is carried out. If the right-hand side of Eq. (3) consisted only of Q, then Q and HS would be exactly 90° out of phase. Comparing Fig. 3 upper-left and upper-right panels, it can be seen that both the HS increase in winter–spring and decrease in summer–autumn are faster than expected if HS were controlled only by Q; therefore, advection and diffusion through the Otranto Channel affect the heat storage significantly. This is again evidence that the inflow of surface and intermediate waters through the Otranto Channel is important for the overall heat budget of the basin.

We have computed the monthly mean freshwater balance and its components evaporation (E), precipitation (P), and river runoff (R). Figure 3 and Table 3 summarize these results. Evaporation data and standard deviations have been determined from the latent heat fluxes of Table 1. Precipitation has been extracted from the climatology developed by Legates and Willmott (1990), who estimated that P is affected by a 40% standard deviation on average. The river discharges have been taken from Raicich (1994), who estimated the standard deviation to be 30%–60%, which is compatible with the estimate for P given above. The error bars for the total water budget, shown in Fig. 3, are then obtained from the individual standard deviations. The three components of the freshwater balance are of the same order of magnitude, with negative values of $E - (P + R)$ in all the months, and a total fresh water gain of 1.14 ± 0.20 m yr^{-1}. The precipitation budget appears to be overestimated probably due to the lack of open sea observations, since precipitation is expected to be lower in the open ocean than along the coasts. We have checked the precipitation data utilized with those observed at coastal stations; it turns out that the Legates and Willmott (1990) data appear to be overestimated as much as 50% along the southeastern coastlines. However, computing the average annual water budget $E - (P + R)$ from the coastal data, the water balance remains negative.

TABLE 3. Freshwater balance components: E is evaporation, P precipitation, and R runoff. All units are in meters.

Month	E	P	R	$E - (P + R)$
Jan	0.14 ± 0.01	0.11 ± 0.05	0.12 ± 0.05	-0.08 ± 0.07
Feb	0.14 ± 0.01	0.09 ± 0.04	0.12 ± 0.05	-0.07 ± 0.06
Mar	0.12 ± 0.01	0.09 ± 0.04	0.12 ± 0.05	-0.09 ± 0.06
Apr	0.11 ± 0.01	0.07 ± 0.03	0.14 ± 0.06	-0.10 ± 0.06
May	0.07 ± 0.01	0.07 ± 0.02	0.13 ± 0.05	-0.13 ± 0.06
Jun	0.05 ± 0.01	0.05 ± 0.02	0.11 ± 0.04	-0.12 ± 0.05
Jul	0.03 ± 0.01	0.03 ± 0.01	0.06 ± 0.03	-0.06 ± 0.03
Aug	0.03 ± 0.01	0.04 ± 0.02	0.05 ± 0.02	-0.06 ± 0.03
Sep	0.04 ± 0.01	0.08 ± 0.02	0.06 ± 0.03	-0.10 ± 0.04
Oct	0.13 ± 0.01	0.12 ± 0.04	0.08 ± 0.03	-0.08 ± 0.05
Nov	0.14 ± 0.01	0.14 ± 0.05	0.13 ± 0.05	-0.13 ± 0.07
Dec	0.18 ± 0.01	0.14 ± 0.06	0.15 ± 0.06	-0.11 ± 0.08
Year	1.17 ± 0.03	1.02 ± 0.12	1.29 ± 0.16	-1.14 ± 0.20

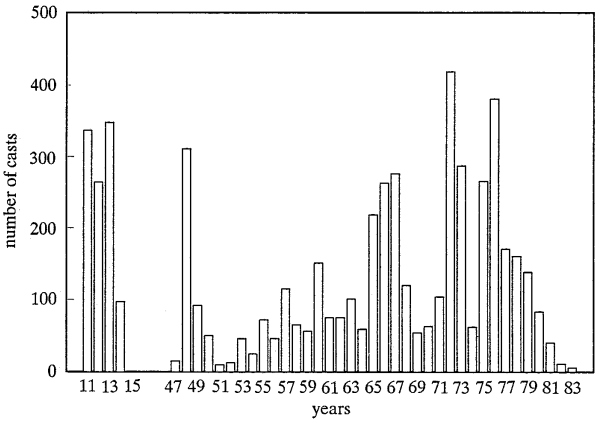

FIG. 4. Yearly cast distribution.

3. The hydrographic dataset

The hydrographic dataset comprises measurements of temperature, salinity, and dissolved oxygen taken by bottle sampling in the periods 1911–14 and 1947–83. The yearly station distribution is shown in Fig. 4. After 1983 all the measurements were made with CTD casts, which will be considered in a following paper. All the stations with less than 15-m bottom depth and others located close to the eastern coast have been omitted from our analysis since we wanted to eliminate water properties strongly affected by coastal processes. The resulting dataset comprises a total of 5543 stations (Table 4), 5518 of which include temperature, 5503 include salinity, and 2673 include dissolved oxygen. Figure 5 shows the spatial distribution of these stations.

Generally, observations were made at the following depths: 0, 5, 10, 20, 30, 40, 50, 75, 100, 150, 200, 250, 300, 400, 500, 600, 800, 1000, and 1200 m. If a value was not available for one of the above depths, linear interpolation between adjacent values was performed.

Most of the data (85%–90%) was obtained from hydrological casts performed by Nansen and Niskin bottles (or other analogous bottles) equipped with protected and unprotected reversing thermometers. The uncertainty on the percentage is due to the fact that some authors used both reversing thermometers and in situ probes, but they did not specify in their papers from which instrument the data were obtained.

Until 1960 salinity data were obtained by means of the Mohr–Knudsen titration method, using the *Eau de Mer Normale* as standard. After 1970, all of the salinity determinations were made from laboratory salinometers calibrated with the same standard. Between 1960 and 1970, many authors used both methods in conjunction. The authors rarely gave confidence limits of the experimental data. We can assume that the approximate temperature uncertainty is 0.02°C and for salinity it is 0.02 psu for titration and 0.005 psu for the conductivity method. More details can be found in U.S. Navy (1968).

The analytical method usually adopted for the dissolved oxygen determination is outlined by Winkler (1888). Various adaptations, essentially concerning the standardization procedures, have been reported by Jacobsen (1921), Vercelli and Picotti (1926), Thompson and Robinson (1939), and Koide, quoted in Trotti (1969). After 1960 the methodology follows the suggestions proposed by Strickland and Parsons (1960), except for some improvements in the standards as reported by Grasshoff et al. (1983). The authors rarely report experimental accuracy and sensitivity limits; therefore, we rely on the description of each method. Generally, both accuracy and sensitivity cannot be considered better than 0.05 ml l^{-1}.

The following quality checks were carried out on the raw dataset: (i) geographical position check; (ii) check that the same station did not appear in different datasets; (iii) climatological check, which consists of the follow-

TABLE 4. Details on the historical Adriatic dataset: C represents the number of casts reported in each reference; C_T the number of casts with temperature data; D_T the number of temperature data; C_S, D_S, the same for salinity; and C_O, D_O the same for dissolved oxygen.

Reference	C	C_T	D_T	C_S	D_S	C_O	D_O
Artegiani and Azzolini (1980)	107	107	640	107	644	40	284
Artegiani et al. (1981)	115	115	450	115	455	115	450
Brasseur et al. (1993)	850	832	4492	832	4212	338	1669
Brückner (1912, 1913, 1915)	350	350	2345	348	2340	92	174
Buljan and Zore-Armanda (1966, 1979)	1062	1061	8042	1051	7955	322	2668
Cescon and Scarazzato (1979)	523	523	1974	523	1971	392	1341
ENEA (1990)	583	583	2513	581	2499	—	—
Franco (1970, 1972, 1982)	335	335	1398	335	1415	320	1355
Hydrographic Inst. of the Yugoslav Navy (1982)	154	154	1566	154	1566	133	1283
Inst. za Oceanologiju i Ribarstvo, Split (1985)	29	29	175	29	171	16	29
Levitus (1982)	129	129	808	129	816	49	348
P. Malanotte-Rizzoli (1972, pers. comm.)	73	73	431	73	427	73	425
Mosetti and Lavenia (1969)	300	300	1788	300	1787	—	—
R. Comitato Talassografico (1912, 1913, 1914)	471	470	4050	470	4050	373	1587
Trotti (1969)	171	171	1239	171	1238	171	1173
Zore-Armanda et al. (1991)	291	286	2866	285	2809	239	2419
Total	5543	5518	34 777	5503	34 355	2673	15 205

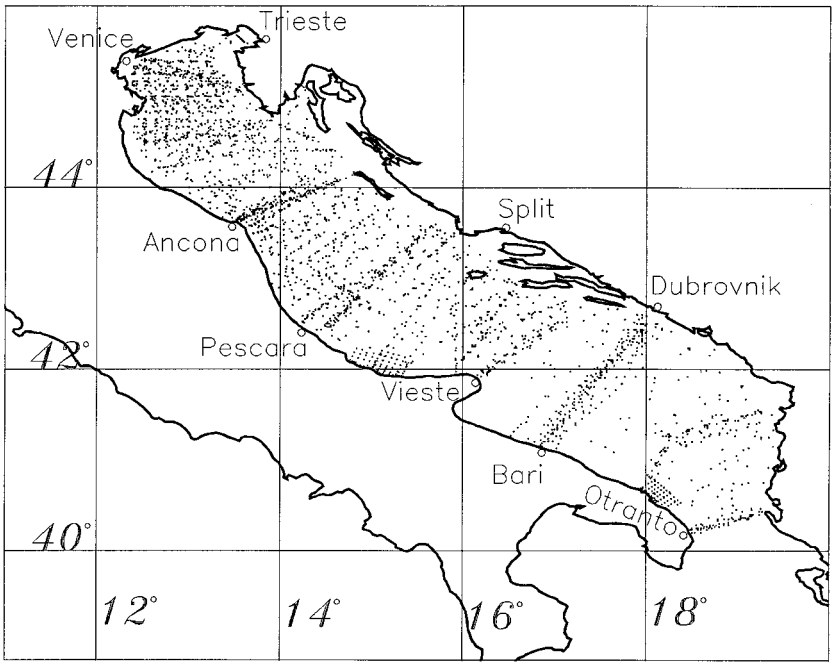

FIG. 5. Spatial cast distribution.

ing: Since the data exhibit large spatial and temporal variability, the Adriatic Sea was divided into six areas for which the monthly means and standard deviations were calculated. For temperature and salinity the measurements were averaged in the following layers: 0–9 m, 10–29 m, 30–99 m, 100–269 m, 270–599 m, and from 600 m to the bottom. All of the values that departed from the mean by more than three standard deviations were rejected. For dissolved oxygen every depth was examined separately in each area. All of the values outside the range 4.5–6 ml l^{-1} and departing from the mean by more than three standard deviations were rejected. This procedure was repeated three times, discarding 202 values of dissolved oxygen.

On the basis of the climatological averages of these data, we defined three regions with homogeneous physical water properties: the northern Adriatic extending up to the 100-m isobath in the south, the middle Adriatic characterized by the Pomo Depressions up to the Vieste transect, and the southern Adriatic up to the Otranto Channel. The northern Adriatic region is slightly larger than previously defined (Orlić et al., 1992) because we found that the water properties are homogeneous when calculated according to the regional boundaries defined here.

4. Water mass structure

a. Temperature and salinity

Figures 6, 7, and 8 show the climatological profiles for temperature and salinity and the climatological TS diagrams obtained from our dataset for the three regions defined above. In the following we describe the water mass characteristics of the three regions separately.

In the northern Adriatic the entire water column exhibits an evident seasonal thermal cycle. A well-developed thermocline is present in spring and summer down to 30-m depth, whereas a significant cooling begins close to the surface in autumn when the bottom temperature reaches its maximum value, probably due to increased vertical mixing and intrusion of middle Adriatic waters. Only in winter the cooling of the whole water column occurs; in this season temperature generally increases down to the bottom, but the water column stability is preserved due to an associated increase of salinity at depth. The freshwater effect is clearly seen in spring and summer due to the increased runoff and the increased water column stratification. From these averaged temperature and salinity profiles there is no evidence of modified Levantine Intermediate Water (MLIW) (described later for the middle Adriatic) in the northern basin. We can recognize a seasonal layer of northern Adriatic surface water (NAdSW), which corresponds to low salinities and relatively high temperatures of the summer, and a northern Adriatic deep water (NAdDW) layer, which is cooled and renewed in winter. From Fig. 8a we can define the NAdDW having average characteristics of $T = 11.35 \pm 1.40$°C, $S = 38.30 \pm 0.28$ psu, and density $\sigma_t > 29.2$ kg m^{-3}.

In the middle Adriatic the spring–summer thermocline is formed down to a depth of 50 m. In the layer from 50 to 150 m the seasonal temperature changes are still observed. The MLIW in this region is defined by

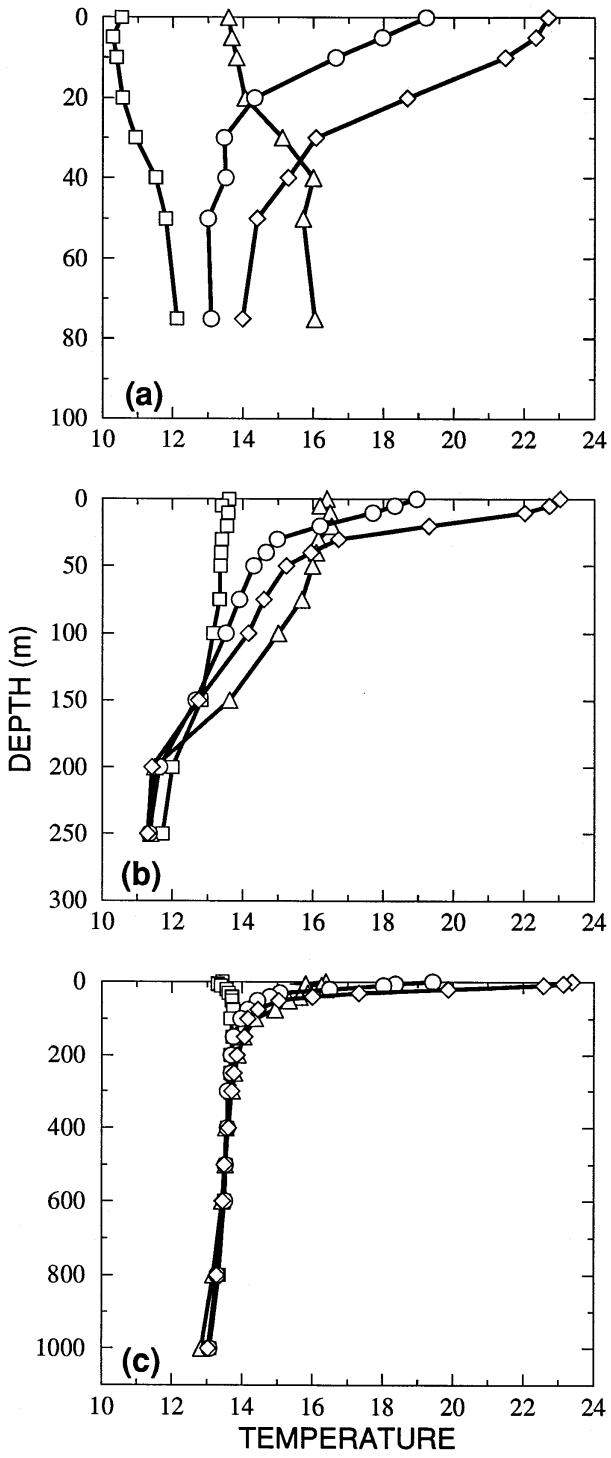

FIG. 6. Seasonal climatological profiles of temperature (°C) for (a) northern, (b) middle, and (c) southern Adriatic for winter (□), spring (○), summer (◇), and autumn (△).

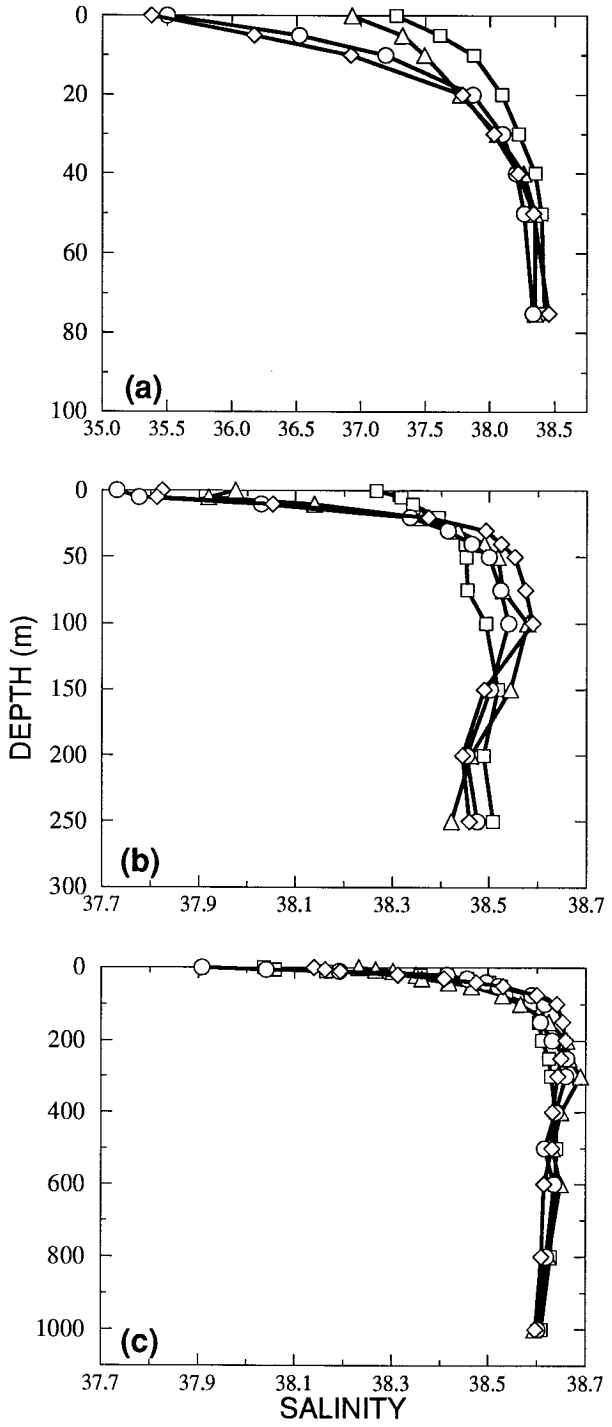

FIG. 7. Seasonal climatological profiles of salinity (psu) for (a) northern, (b) middle, and (c) southern Adriatic for winter (□), spring (○), summer (◇), and autumn (△).

waters with salinity $S > 38.5$ psu below 50 m. The surface waters are freshened during spring and summer, as in the northern Adriatic, due to river runoff. Hence, the river runoff also exceeds evaporation during summer in the middle Adriatic. The Pomo Depressions are the only areas deeper than 150 m. They are filled with a deep water mass, which exhibits some seasonal changes. The middle Adriatic deep water (MAdDW) has relatively low average temperature ($T = 11.62 \pm 0.75$°C) and substantially higher

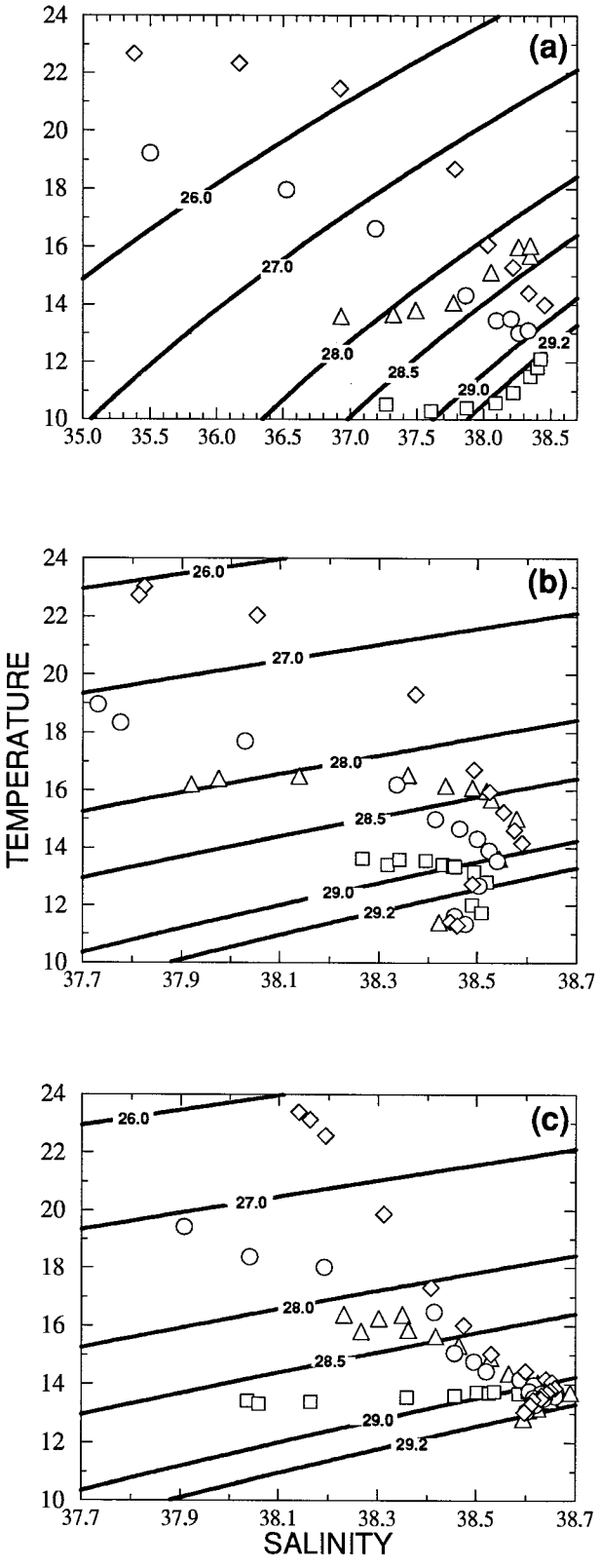

FIG. 8. Climatological *T*–*S* diagram for (a) northern, (b) middle, and (c) southern Adriatic for winter (□), spring (○), summer (◇), and autumn (△). The solid lines indicate σ_t.

average salinity ($S = 38.47 \pm 0.15$ psu) than the NAdDW but the density is still $\sigma_t > 29.2$ kg m^{-3}, Fig. 8b. If this water originates from the winter NAdDW moving southward, then it experiences substantial mixing and entrainment, transforming the NAdDW into MAdDW. From spring to autumn, the MAdDW is the coldest bottom water mass in all the Adriatic basin.

In the southern Adriatic the seasonal thermocline extends down to approximately 75 m. The seasonal cycle of the surface waters is driven by the fresh coastal waters as seen by the decrease in salinity in all seasons and the augmented minimum during spring and summer. From 150 m to the bottom, Mediterranean open sea conditions are found since the water is almost homogeneous, with a relatively weak seasonal signal down to 300 m, modulated by MLIW advection and mixing. In this region the MLIW is defined by $S > 38.6$ psu and $T > 13.5$°C, with a layer between 150 and 400 m. The southern Adriatic deep water (SAdDW) again has different average characteristics from NAdDW and MAdDW. It is defined by $T = 13.16 \pm 0.30$°C and $S = 38.61 \pm 0.09$ psu, corresponding to $\sigma_t > 29.1$ kg m^{-3} (Fig. 8c). Thus, this water is considerably warmer and saltier compared to NAdDW and MAdDW so that it probably comprises a mixture of MLIW and local surface waters (Ovchinnikov et al. 1985; Roether and Schlitzer 1991).

To quantify the variability of the hydrological parameters we use the observed standard deviations (STD) associated with the climatological mean values. The STDs depend mainly on the seasonal and interannual fluctuations but are also strongly affected by the number of observations used in the computations.

In the northern Adriatic temperature STD ranges from 0.8°–1.1°C near the bottom (with a minimum value in spring and a maximum in winter) to 2.1°–2.6°C near the surface (a minimum in winter and maximum in autumn). In spring and summer the maximum respective STDs 2.2° and 2.4°C occur at 20 m as a consequence of the variability in the thickness of the seasonal surface mixed layer. In the middle Adriatic the temperature STD is 0.6°–0.8°C near the bottom and ranges between 1.1°C in winter and 2.4°C in spring near the surface. In this region the highest variability in the summer occurs at 20-m depth (STD = 1.9°C), as in the northern basin. In the southern Adriatic, the bottom STD is about 0.2°C, while at the surface it ranges between 1.1°C in winter and 2.5°C in spring. Again the maximum summer STD occurs at 20 m (STD = 2.3°C).

The salinity STD always decreases from the surface to the bottom in all three subbasins. In the Northern Adriatic the lowest STDs range from 0.1 psu in winter and 0.3 psu in summer, near the bottom, and the highest from 2.1 psu in autumn to 3.2 psu in spring at the surface. The middle Adriatic winter salinity exhibits the lowest variability, with STD of 0.1 psu near the bottom and 0.5 at the surface, while the other seasons are similar to each other, with bottom STD of 0.2 psu and surface STD of 0.9–1.1 psu. In the southern Adriatic the bottom

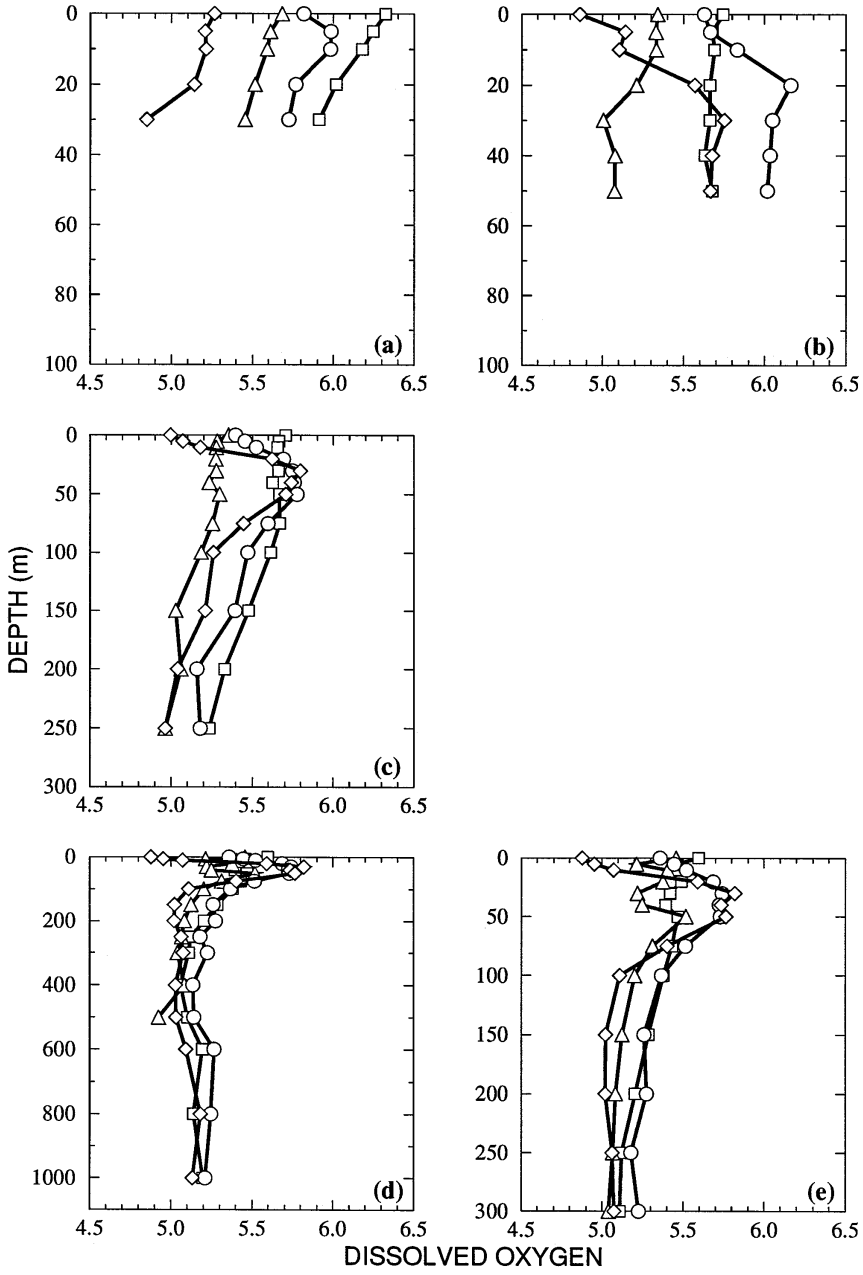

FIG. 9. Climatological profiles of dissolved oxygen (ml l^{-1}) for (a) the northern Adriatic with bottom depth less than or equal to 50 m, (b) northern Adriatic with bottom depth greater than 50 m, (c) middle Adriatic, (d) southern Adriatic for the entire water column, and (e) southern Adriatic for the upper 300 m. Symbols indicate winter (□), spring (○), summer (◇), and autumn (△).

STD is less than 0.1 psu, whereas at the surface it ranges between 0.3 psu in summer and 0.8 psu in spring.

b. Dissolved oxygen

The whole Adriatic Sea is a well-oxygenated basin. The dissolved oxygen profiles (Fig. 9) show that in the warmer seasons a relatively low concentration layer is present just near the sea surface, due to oxygen equilibration with the atmosphere. During spring and summer a subsurface maximum is formed in the euphotic zone, between approximately 10 and 50 m, due to biological activity that results in a net production of oxygen near the pycnocline after the density stratification of the water column has become established. In autumn and winter ventilation at the surface and water column mixing create a more homogeneous oxygen distribution.

In the northern Adriatic we noticed a qualitatively

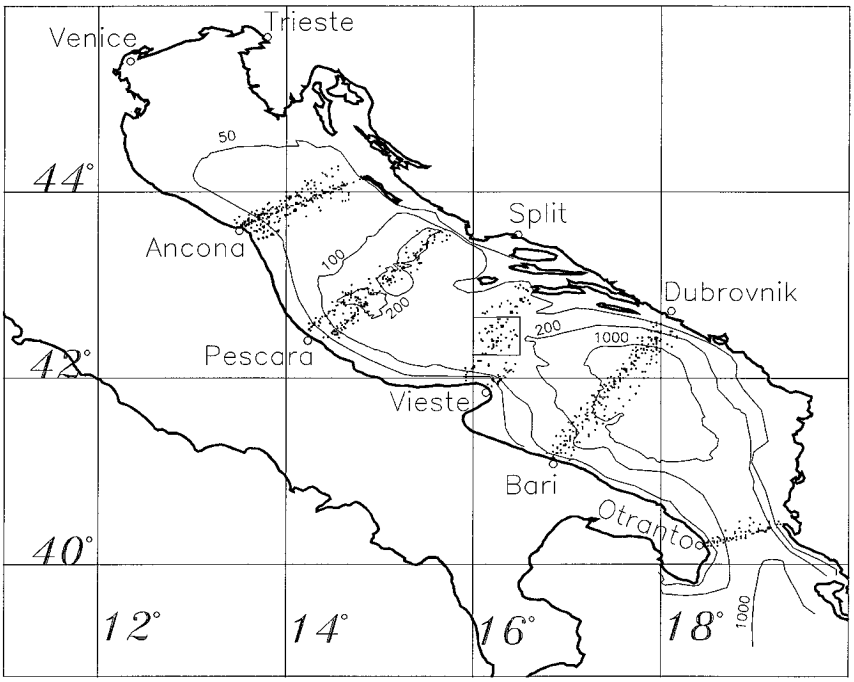

FIG. 10. Spatial cast distribution along selected cross sections. The Pelagosa area is indicated by the box on the Vieste section.

different shape of the average oxygen profiles with respect to middle and southern Adriatic conditions, and thus we subdivided the northern Adriatic in two subregions. The first corresponds to the area shallower than 50 m, called NA-I region, and the second corresponds to the remaining part, called NA-II region. In Fig. 9a for the NA-I region, we show that in all seasons there is no subsurface oxygen maximum except for spring when we observe it at 5–10 m. The NA-II region by contrast shows maximum subsurface values for spring and summer as for the middle and southern Adriatic cases. Naturally, the highest values of oxygen for the entire basin are reached during winter in the NA-I region. Thus, the NA-I region is clearly that part of the northern Adriatic basin that is characterized by shallow sea dynamics evidenced by the increased mixing throughout the water column, even during summer. In contrast deep-sea conditions are found in the NA-II region where oxygen profiles look similar to those of the middle Adriatic. Hence, the pelagic lower trophic system dynamics (i.e., nutrients and phytoplankton) are expected to be different in NA-I and NA-II regions based on different vertical distributions of oxygen.

In the middle Adriatic the oxygen concentration decreases from the euphotic zone (50 m) down to the bottom, while in the southern Adriatic a minimum is found at 150–250 m due to the organic matter oxidation. Below this minimum, the oxygen concentration slightly increases down to the bottom. The relative minimum at 40–50 m in autumn and winter in the southern Adriatic (Fig. 9d) could be due to fewer observations relative to the levels above and below those depths.

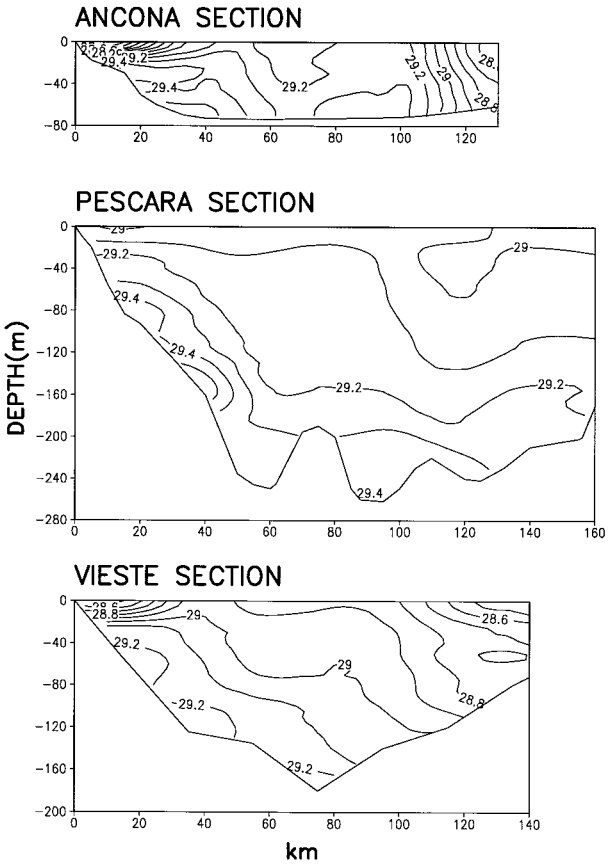

FIG. 11. Sigma-t anomaly (kg m^{-3}) vertical distribution along the Ancona, Pescara, and Vieste sections for winter.

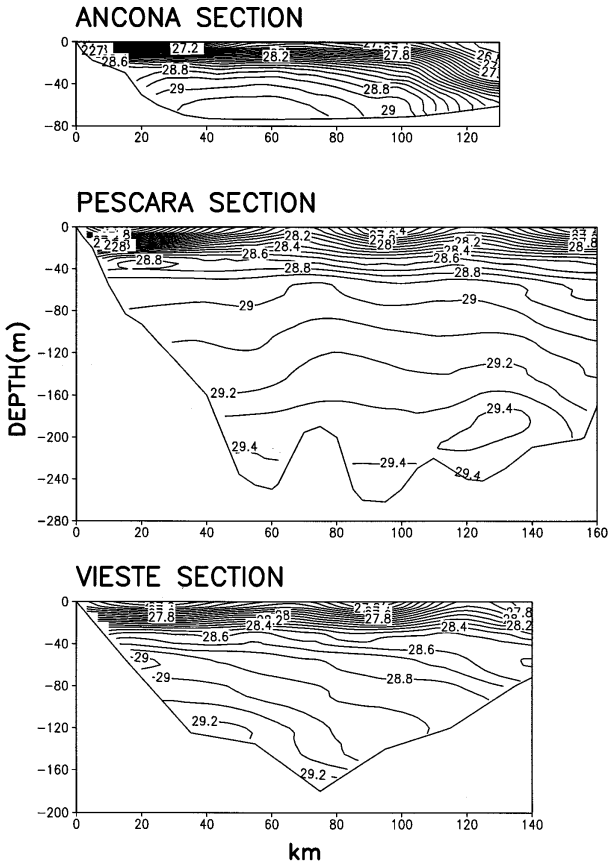

FIG. 12. Sigma-t anomaly (kg m^{-3}) vertical distribution along the Ancona, Pescara, and Vieste sections for spring.

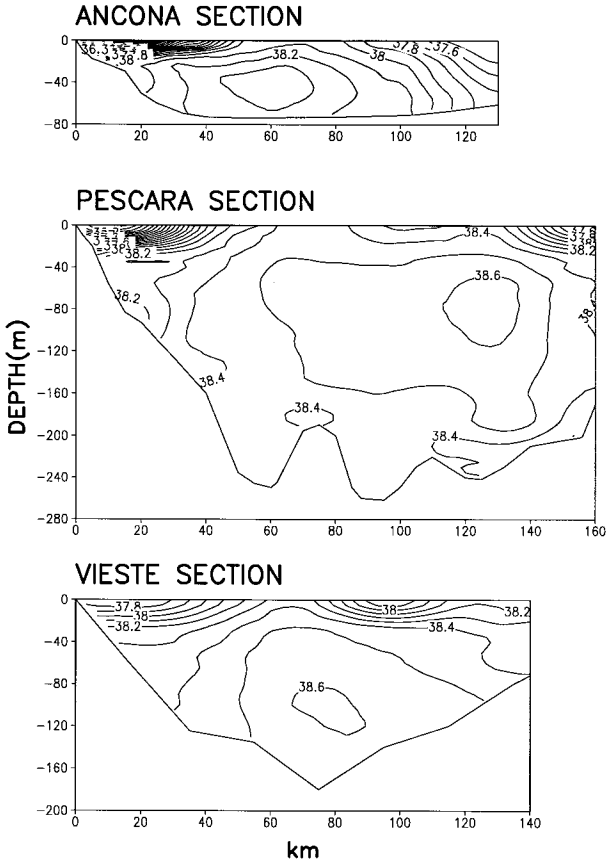

FIG. 13. Salinity (psu) vertical distribution along the Ancona, Pescara, and Vieste sections for spring.

An average basin value of dissolved oxygen is approximately 5.5 ml l^{-1}, and we used standard deviations (STD) to describe the oxygen variability. In the northern Adriatic the lowest variability in the oxygen concentration occurs near the bottom with STD ranging from 0.1 ml l^{-1} in autumn and 0.4 ml l^{-1} in summer, while the highest STDs occur at the surface with values of 0.5–0.6 ml l^{-1} in all seasons except for summer when the highest STD of 0.9 ml l^{-1} is found at a depth of 30 m. In the remaining part of the Adriatic Sea STD exhibits neither significant seasonal changes nor a clear dependence on the depth. In the middle Adriatic the STD range is 0.3–0.6 ml l^{-1}, and in the southern basin where the number of observations is relatively low along the entire water column the STD mainly ranges between 0.2 and 0.4 ml l^{-1}.

Usually, the oxygen saturation percentage does not drop below 75%, whereas maximum values can be greater than 110%. In the northern Adriatic hypoxia (mostly deduced from phenological observations but rarely measured) can occur under particular conditions associated with specific phenomenology. Such occurrences cannot be recognized in our mean values due to the sporadic nature of these events.

5. Vertical sections

In this section we describe the seasonal variability in temperature, salinity, and density for five lateral sections. The station locations that define the sections are shown in Fig. 10. We see that along these five sections the stations accumulate so that it is possible to define seasonal mean properties along an average position, which we call a section. The sections are called Ancona, Pescara, Vieste, Bari, and Otranto after the nearby Italian cities.

a. Ancona, Pescara, and Vieste sections

The Ancona section is representative of the transition area between the northern and middle Adriatic regions. The Pescara section characterizes the middle Adriatic, while the Vieste section represents the transition area to the southern Adriatic.

The density distribution on these three sections is shown in Fig. 11 for winter and Fig. 12 for spring. Two important characteristics of the northern and middle Adriatic winter circulation are evident from Fig. 11; (i) the coastal waters affected by river runoff are confined along the continental shelf and escarpments of both

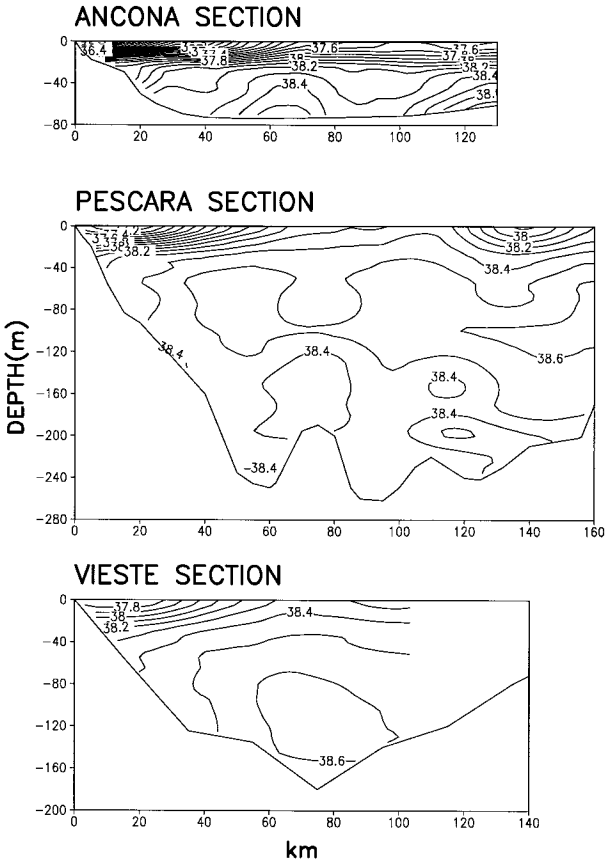

FIG. 14. Salinity (psu) vertical distribution along the Ancona, Pescara, and Vieste sections for summer.

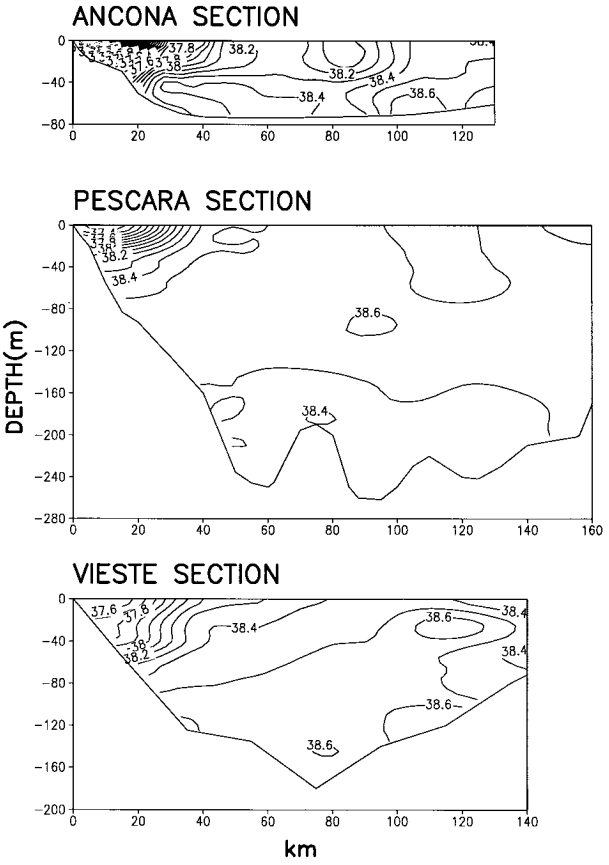

FIG. 15. Salinity (psu) vertical distribution along the Ancona, Pescara, and Vieste sections for autumn.

sides of the Adriatic basin and (ii) the NAdDW and MAdDW are traceable in all the sections.

At the Ancona section the NAdDW ($\sigma_t > 29.2$ kg m^{-3}) occupies the deepest part of the section and the heaviest core of waters is found along the Italian escarpment. At the Pescara section, two distinct nuclei of dense waters occur: the first hugs the Italian escarpment and is probably still identifiable as NAdDW; the second is characterized as MAdDW filling the Pomo Depressions. At the Vieste section, the MAdDW is largely diluted with respect to the Pescara section but it is still evident in ''blobs'' along the Italian escarpment.

During spring (Fig. 12) the NAdDW is absent from the Ancona section and only a core of water with $\sigma_t \approx$ 29.1 kg m^{-3} occupies the central bottom region. The MAdDW preserves its properties even during spring and thus from spring to autumn it becomes the heaviest water of the Adriatic basin. The Pomo Depressions isolate this MAdDW from neighboring water types. At the Vieste section and during the spring the MAdDW is still present in two small cores of waters along the Italian escarpments and Pomo Depressions. Our results are consistent with the conclusions drawn by many previous authors. A dense water pool is reported to be found in winter in the northern Adriatic by Hendershott and Rizzoli (1972), Malanotte-Rizzoli (1977), and Artegiani et al. (1989). In agreement with our analysis, Franco and Bregant (1983), Artegiani and Salusti (1987), and Artegiani et al. (1989) show that the NAdDW flows along the western coast of the basin and subsequently fills the Pomo Depressions. From our analysis evidence is found for a seasonal residence time of the NAdDW in the Northern and Middle Adriatic. Also it can be concluded that climatologically the MAdDW is renewed annually in the Pomo Depressions by NAdDW flowing southward. Local formation of dense water in the middle Adriatic has also been reported by Zore-Armanda (1963).

The other characteristics of the northern and middle Adriatic circulation are examined using the salinity sections shown in Figs. 13, 14, and 15. During spring the low salinity waters are still confined along the lateral sides of the basin in all the sections with the possible exception of Vieste. During summer the low salinity waters induced by river runoff extend throughout the surface layers of the sections. The lowest salinity waters are, however, always confined along the western shelf area of the basin, both at the Pescara and Vieste sections. The autumn conditions, shown in Fig. 15, represent the

transition toward the wintertime regime with increased gradients of salinity along the escarpments.

At intermediate depths between 50 and 150 m we can detect (in Figs. 13, 14, and 15) the presence of MLIW ($S > 38.5$ psu in the middle and $S > 38.6$ psu in the southern Adriatic) in all seasons except winter (not shown). The greatest intrusion of MLIW is evident in autumn, as shown by the large area enclosed by the 38.5-psu isohaline in Fig. 15 for the Pescara and Vieste sections. At the Ancona section the MLIW can be traced on the eastern side of the section only during summer and autumn. The MLIW did not result from the average climatological profiles of Fig. 8a since the area occupied by this high salinity water mass is relatively small and the spatial average removes this signal.

b. Bari section

This section is representative of the central southern Adriatic. The winter conditions, shown in Fig. 16a, are characterized by low temperature and low salinity coastal waters on the western shelf area of the Adriatic. In the deepest part of the section we find the SAdDW with $T < 13.0$°C and $S < 38.6$ psu. These dense waters are probably of local origin, in agreement with the results by Pollak (1951), Ovchinnikov et al. (1985), and Roether and Schlitzer (1991), who indicate the southern basin as an area of SAdDW formation. Above the SAdDW there is a thick transition layer with $13.0 < T < 13.5$°C, and the MLIW lies above that layer.

During spring (Fig. 16b), the MLIW is evident only on the eastern side of the basin and it exhibits patchiness at intermediate depths. The SAdDW is still evident at the bottom while the surface waters have decreased their salinity in the first 50 m. Hence, we conclude again that the river runoff waters affect also the southern Adriatic surface waters.

c. Otranto section

This section is shown in Fig. 17 for winter and spring conditions. This is the route of exchange of waters with the eastern Mediterranean, so that it is interesting to trace the deep water masses along the section.

During winter, the western side of the section along the escarpment is occupied by a very dense water characterized by $T < 13.5$°C and $S < 38.6$ psu. The central and eastern part of the section shows the presence of MLIW ($13.5° < T < 14.5$°C, $S > 38.6$ psu). The SAdDW is evident as a small nucleus in the deepest part of the section with $T \approx 13.5$°C and $S \approx 38.6$ psu.

During spring the MLIW central core is shifted upward around 300 m, while during winter it is centered around 600 m. It is interesting to note that during spring the SAdDW seems to have cooled and freshened a little with respect to winter values. Thus, we conclude that the SAdDW could have mixed with MAdDW and/or the heavy coastal waters seen along the western escarpment during winter. However, the paucity of data in this region of the Adriatic does not allow us to draw any definitive conclusions about mixing of different water masses in the Southern basin.

6. Interannual variability of time series

The entire dataset presented here contains few areas with long time series. We choose to show the time series in a region of 36×41 km^2 at the center of the Vieste section. This area is called Pelagosa after the nearby island. Between 1947 and 1983 we have temperature and salinity data with the exception of 1951–52 and 1973–74.

In Figs. 18a,b we show the area-averaged temperature and salinity anomalies for the surface and 100-m depth after the seasonal cycle has been removed. As expected, the temperature interannual variability is larger at the surface, with maximum deviations of 4°C, than at depth (deviations of 2°C at 100 m). The analysis by means of the periodogram method (Stull 1988) reveals that the interannual variability in temperature and salinity peaks at different periods. Temperature anomalies are dominated by fluctuations of high frequency (1–2 yr) and relatively low frequency (12–13 yr) both at the surface and 100 m. The variance explained by the 1-yr and 2-yr fluctuations is about 10% at both levels, and the 12-yr or 13-yr components explain about 7% of total variance at the surface and 13% at 100 m. The variability of salinity anomalies is characterized by fluctuations of intermediate frequency (3 and 6 yr), both at the surface and at 100 m. At 100 m a 12-yr fluctuation is also found, as for temperature at that depth. The 3-yr and 6-yr components explain about 9% and 18%, respectively, of the time series variance at the surface, while at 100 m approximately 15% of the total variance is explained by the 12-yr component, 8% by the 6-yr component, and 6% by the 3-yr component. Since 1970–71 we can detect a trend of increasing salinity and temperature but the data are not sufficiently accurate to make conclusions about climatic changes (Zore-Armanda et al., 1991).

7. Conclusions

The work presented here describes the climatological water mass and dissolved oxygen structure of the Adriatic Sea. The dataset was collected and quality-controlled and a seasonal climatological analysis produced. A monthly analysis was not feasible because of the paucity of data.

First, we studied the meteorology of the basin and the air–sea interaction budgets. Several climatological wind datasets were compared and discussed and the climatological heat budget of the basin computed by means of bulk formulas. The heat budget at the surface is dominated by the incoming shortwave heat flux balanced by longwave and latent heat energy losses. It was

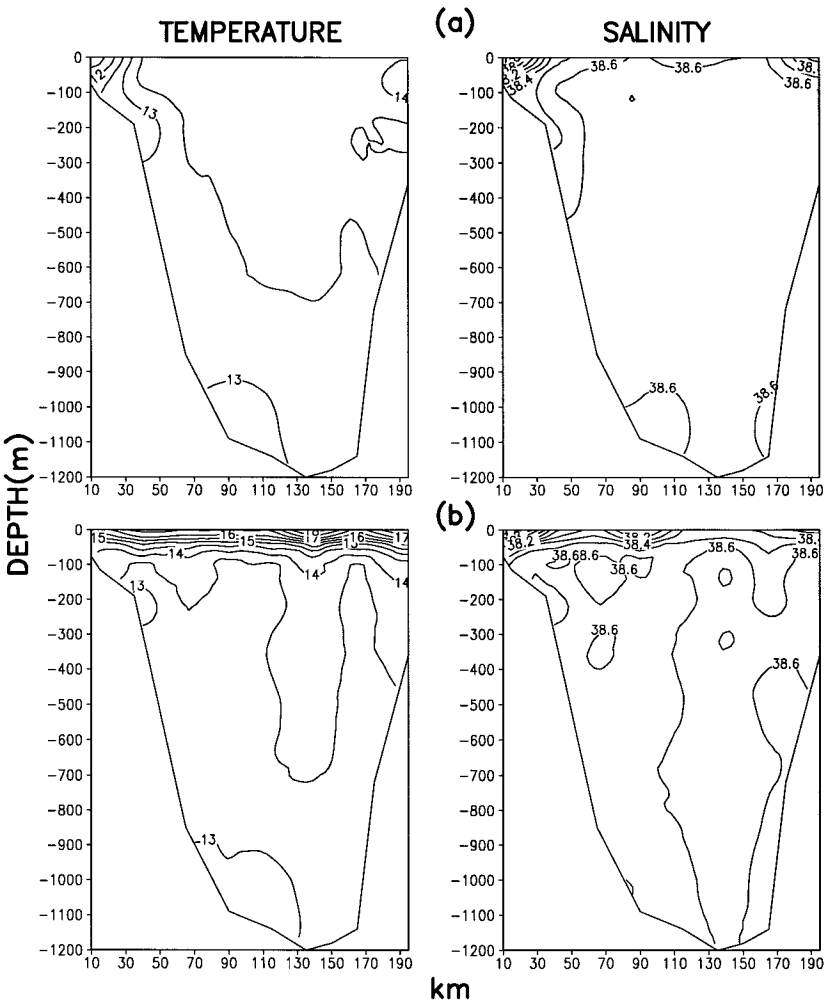

FIG. 16. Temperature (°C, left) and salinity (psu, right) vertical distributions along the Bari section for (a) winter and (b) spring.

found that the basin has an overall long term heat loss of 19–22 W m^{-2}, which implies an import of heat from the northern Ionian through the Otranto Channel. The latter is shown to play an important role also in the heat storage balance of the Adriatic basin. These climatological considerations show that the Adriatic is a heat engine like the overall Mediterranean, but it is a dilution basin since the freshwater balance implies an average freshwater gain of 1.14 m yr^{-1}.

The overall Adriatic basin is subdivided in three areas: the Northern basin with shallow sea water mass characteristics; the middle Adriatic, which is a transition basin but with some well-defined open sea characteristics (persistence of a pool of deep water during spring–summer seasons); and the Southern basin with open sea water mass characteristics below 150 m.

We have classified for the first time the water masses of the basin using climatological averages and vertical sections. The surface waters of all the three regions undergo a clear temperature seasonal cycle with maximum values of temperature during summer and maximum mixed layer depths during winter. The salt balance of the surface layer is clearly affected by freshwater river runoff in all the three regions during spring and summer. Fresher coastal waters are always separated and distinguishable from open sea waters in all seasons. We can recognize the MLIW and deep waters spreading paths. The MLIW is defined by $S > 38.5$ psu in the middle Adriatic and $S > 38.6$ psu in the subsurface layers of the southern Adriatic. Its maximum abundance is reached during autumn where it occupies almost the entire water column in the middle and southern Adriatic. The MLIW intrusion can be detected also in the northern Adriatic, but from the climatology we have no evidence of such a phenomenon, which seems to be rather localized. To a first-order approximation the northern Adriatic seems to be dynamically independent of the middle and southern Adriatic, however, it clearly influences the dynamics of the other two regions through the southward movement of NAdDW.

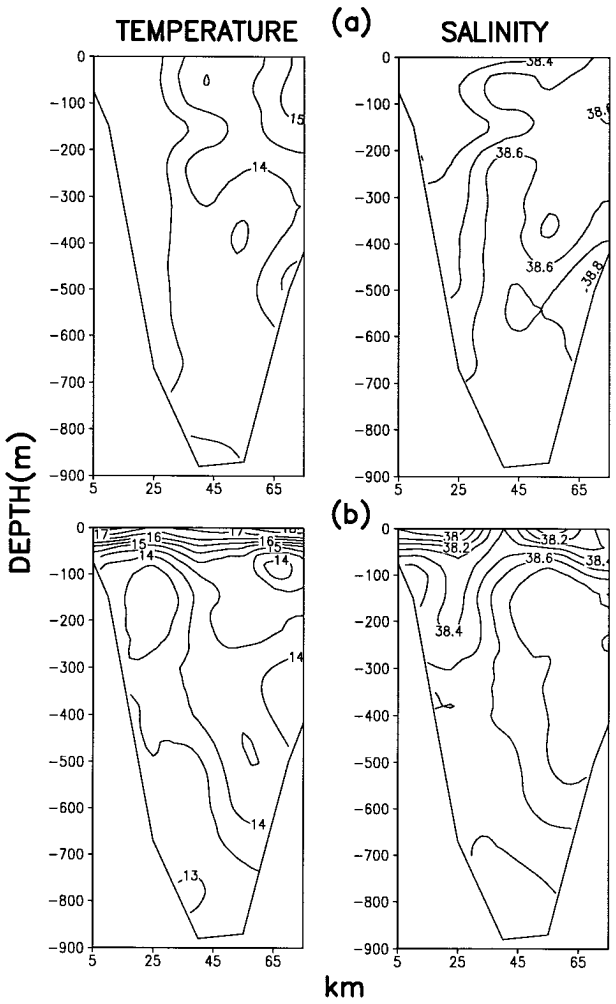

FIG. 17. Temperature (°C, left) and salinity (psu, right) vertical distributions along the Otranto section for (a) winter and (b) spring.

The deep waters of the Adriatic can be separated into two categories: the first, clearly formed in the northern Adriatic region, cool and relatively fresh, found in the northern and middle Adriatic, and the second of much higher temperature and salinity, in the southern Adriatic. It is our perception that vertical mixing between water masses is an extremely powerful dynamical process in the basin, especially as an explanation of the modification of NAdDW into MAdDW.

Acknowledgments. This research has been undertaken in the framework of the Mediterranean Targeted Project (MTP)—MERMAIDS II Project, and finished during the Mediterranean Targeted Project phase II—MATER. We acknowledge the support of the European Commission's Marine Science and Technology Programme (MAST II and III), Contracts MAS2-CT93-0055 and MAS3-CT96-0051. We thank Dr. S. Castellari for guidance in the air–sea interaction modeling. We thank also Drs. J. Baretta, P. Radford, and M. Zavatarelli and Prof. G. Mellor for helpful comments on the manuscript. Thanks are also due to Mr. P. Carini for his assistance in figure drawing.

APPENDIX

Heat Budget Computations

The computation of the net heat flux at the sea surface Q has been made by means of the bulk formulas (in SI units), which will be summarized here. More details can be found in CPL97. Here Q can be expressed as

$$Q = Q_S - Q_B - Q_H - Q_E,$$

where Q_S is the downward flux of solar radiation reaching the sea surface, Q_B the net longwave radiation flux emitted from the sea surface, and Q_H and Q_E the sensible and latent heat fluxes from the sea surface to the atmosphere.

The incident solar radiation flux Q_S can be written as

$$Q_S = Q_{\text{TOT}} (1 - 0.38\ C - 0.38C^2) (1 - \alpha),$$

where C is the fractional cloud cover and α is the ocean surface albedo, which depends on the solar altitude according to Payne (1972). The cloud attenuation factor was proposed by Berliand (Budyko 1974).

Here Q_{TOT} is the sum of two components, the flux of direct radiation reaching the surface and the flux of radiation scattered downward by the atmosphere

$$Q_{\text{TOT}} = Q_{\text{DIR}} + Q_{\text{DIFF}}$$

$$Q_{\text{DIR}} = Q_0\ \tau^{\text{secz}};$$

$$Q_{\text{DIFF}} = 0.5[(1 - A_a)\ Q_0 - Q_{\text{DIR}}].$$

Here Q_0 is the solar radiation flux at the top of the atmosphere, z the zenith angle, Q_{DIR} is the fraction of Q_0 transmitted through the atmosphere (transmission coefficient $\tau = 0.7$), and Q_{DIFF} is computed under the hypothesis that the radiation scattering in clear sky occurs half downward and half upward (Rosati and Miyakoda 1988); the scattered radiation is the amount not reaching the surface minus that absorbed by water vapor and ozone (absorption coefficient $A_a = 0.09$). The expression for Q_0 is

$$Q_0 = J_0 a^{-2} \cos(z) D_F(\phi),$$

where $J_0 = 1.35 \times 10^3$ J m^{-2} s^{-1} is the solar constant, a the earth radius, and $D_F(\phi)$ the fraction of daylight.

The longwave radiation flux Q_B is computed by means of Berliand's formula (Simpson and Paulson 1979)

$$Q_B = \varepsilon\sigma T_a^4 (0.39 - 0.05 e_a^{1/2})(1 - 0.8C^2) + 4\varepsilon\sigma T_a^3 (T_s - T_a),$$

where $\varepsilon = 0.97$ is the ocean longwave emissivity, $\sigma = 5.67 \times 10^{-8}$ W m^{-2} K^{-4} the Stefan–Boltzmann constant, T_s and T_a the sea and atmosphere temperatures, and C the fractional cloud cover; e_a is the atmospheric vapor

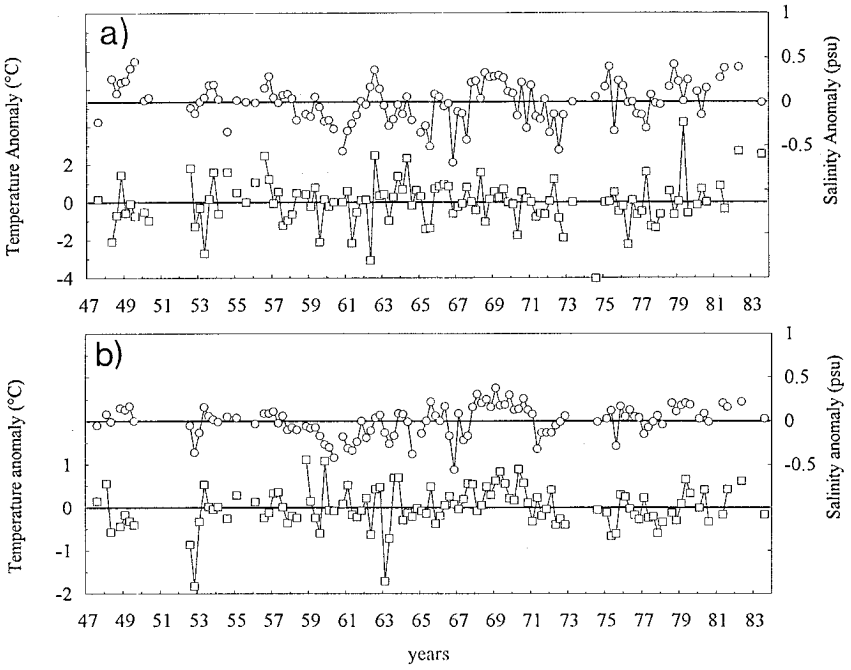

FIG. 18. Temperature and salinity time series for the Pelagosa area at (a) the surface and (b) the 100-m depth.

pressure (hPa) and can be expressed in terms of the saturation vapor pressure e_{sat} and the relative humidity U (%)

$$e_a = 0.01Ue_{\text{sat}}(T_a).$$

The sensible and latent heat fluxes are written as

$$Q_H = \rho_M c_H C_p w(T_s - T_a)$$

$$Q_E = L(T_s)\rho_M c_E w[e_{\text{sat}}(T_s) - 0.01Ue_{\text{sat}}(T_a)]0.622p_a^{-1},$$

where ρ_M is the density of moist air, c_H and c_E the turbulent exchange coefficients, $C_p = 1.005 \times 10^3$ J kg^{-1} K^{-1} the specific heat capacity at constant pressure, w the wind speed, T_s and T_a the sea and air temperature, $L(T)$ the latent heat of vaporization, $e_{\text{sat}}(T)$ the saturation vapor pressure, U the relative humidity, and $p_a = 1013$ hPa the atmospheric pressure. The number 0.622 represents the ratio between the gas constants for dry air R_d and water vapor R_v. The density of moist air is given by

$$\rho_M = 100\frac{p_a}{R_d T_a}\frac{0.622(1 + r_w)}{(0.622 + r_w)},$$

where

$$r_w = 0.01Ue_{\text{sat}}(T_a)0.622{p_a}^{-1}$$

is the mixing ratio.

The turbulent exchange coefficients c_H and c_E are computed according to Kondo (1975). They can be written as

$$c_H = 1.3 \times 10^{-3}f(S_p);\ c_E = 1.5 \times 10^{-3}f(S_p),$$

where S_p is the stability parameter defined as

$$S_p = \frac{s|s|}{|s| + 0.01},$$

with

$$s = (T_s - T_a)w^{-2}.$$

The expressions for $f(S_p)$ are the following:

$$f(S_p) = \begin{cases} 0 & \text{for } S_p \le -3.3 \\ 0.1 + 0.03S_p + 0.9\exp(4.8S_p) & \text{for } -3.3 < S_p < 0 \\ 1.0 + 0.63S_p^{1/2} & \text{for } S_p \ge 0. \end{cases}$$

The latent heat of vaporization is computed by means of the following equation (Gill 1982):

$$L(T) = 2.5008 \times 10^6 - 2.3 \times 10^3(T - 273.15).$$

Error estimate

The following procedure has been adopted in order to estimate the errors on the heat fluxes. First, averages (μ) and standard deviations (σ) are computed for each grid point of the parameter fields used in the calculations, namely, sea surface temperature, air temperature, relative humidity, and wind speed. Let Q be the basin-averaged heat fluxes computed by means of the fields μ for all the parameters. Then, the heat fluxes are computed by using the fields $\mu + \sigma$ and $\mu - \sigma$ for one selected parameter and the fields μ for the others, obtaining Q_+ and Q_-, respectively. An evaluation of the error on the heat fluxes attributed to the error on the

selected parameter is given by the quantity $\alpha = (|Q - Q_+| + |Q - Q_-|)/2$. This procedure is then repeated for each parameter and the values of α so obtained are combined quadratically to estimate the overall error.

REFERENCES

Anati, D. A., 1977: Topics in the physics of Mediterranean seas. Ph.D. thesis, Weizmann Institute of Sciences, Rehovot, Israel, 86 pp. [Available from CNR—Istituto Talassografico di Trieste, viale Romolo Gessi 2, I-34123 Trieste, Italy.]

Artegiani, A., and R. Azzolini, 1980: Rapporto sulle Campagne Idrologiche effettuate nelle acque costiere marchigiane negli anni 1977–1978. *Quad. Lab. Tecnol. Pesca,* **II,** 307–392.

——, and E. Salusti, 1987: Field observation of the flow of dense water on the bottom of the Adriatic Sea during the winter of 1981. *Oceanol. Acta,* **10,** 387–392.

——, R. Azzolini, and E. Paschini, 1981: Unpublished data collected from 1979 through 1981 in the Adriatic Sea. [Available from CNR di Istituto Ricerche sulla Pesca Marittima, largo Fiera della Pesca 1, I-60125 Ancona, Italy.]

——, ——, and E. Salusti, 1989: On the dense water in the Adriatic Sea. *Oceanol. Acta,* **12,** 151–160.

——, M. Gacić, A. Michelato, V. Kovačević, A. Russo, E. Paschini, P. Scarazzato, and A. Smirčić, 1993: The Adriatic Sea hydrology and circulation in spring and autumn (1985–1987). *Deep-Sea Res.,* **40,** 1143–1180.

——, D. Bregant, E. Paschini, N. Pinardi, F. Raicich, and A. Russo, 1997: The Adriatic Sea General Circulation. Part II: Baroclinic circulation structure. *J. Phys. Oceanogr.,* **27,** 1515–1532.

Brasseur P., J.-M. Brankart, and J.-M. Beckers, 1993: Seasonal variability of general circulation fields in the Mediterranean Sea: Inventory of climatological fields (preliminary version). 221 pp. [Available from Université de Liège, GeoHydrodynamics and Environmental Research, Sart Tilman B5, B-4000 Liège, Belgium.]

Brückner, E., 1912: Beobachtungen auf den Terminfahrten S. M. S. Najade im Jahre 1911. Permanente Internationale Kommission für die Erforschung der Adria, Wien, 119 pp. [Available from CNR - Istituto Talassografico di Trieste, viale Romolo Gessi 2, I-34123 Trieste, Italy.]

——, 1913: Beobachtungen auf den Terminfahrten S. M. S. Najade im Jahre 1912. Permanente Internationale Kommission für die Erforschung der Adria, Wien, 114 pp. [Available from CNR - Istituto Talassografico di Trieste, viale Romolo Gessi 2, I-34123 Trieste, Italy.]

——, 1915: Beobachtungen auf den Terminfahrten S. M. S. Najade in den Jahre 1913 und 1914. Permanente Internationale Kommission für die Erforschung der Adria, Wien, 102 pp. [Available from CNR - Istituto Talassografico di Trieste, viale Romolo Gessi 2, I-34123 Trieste, Italy.]

Budyko, M. I., 1974: *Climate and Life.* Academic Press, 508 pp.

Buljan, M., and M. Marinković, 1956: Some data on Hydrography of the Adriatic (1946–1951). *Acta Adriat.,* **VII,** 1–55.

——, and M. Zore-Armanda, 1966: Hydrographic data on the Adriatic Sea collected in the period from 1952 through 1964. *Acta Adriat.,* **XII,** 1–438.

——, and ——, 1976: Oceanographical properties of the Adriatic Sea. *Oceanogr. Mar. Biol. Annu. Rev.,* **14,** 11–98.

——, and ——, 1979: Hydrographic properties of the Adriatic Sea in the period from 1965 through 1970. *Acta Adriat.,* **XX,** 1–368.

Cescon, B., and P. Scarazzato, 1979: Unpublished original data of Adria cruises 1971–1973, 33 pp. [Available from Osservatorio Geofisico Sperimentale, P.O. Box 2011, I-34016 Trieste, Italy. Copy on magnetic tape at CNR di Istituto Ricerche sulla Pesca Marittima, largo Fiera della Pesca 1, I-60125 Ancona, Italy.]

D'Ancona, U., and M. Picotti, 1958: Crociera talassografica adriatica 1955. Relazione Generale. *Archo Oceanol. Limnol.,* **XI,** 211–225.

E.N.E.A., 1990: *Atlante Climatologico del Mare Adriatico.* E.N.E.A, 28 pp.

Ferentinos, G., and N. Kastanos, 1988: Water circulation patterns in the Otranto Straits, eastern Mediterranean. *Contin. Shelf Res.,* **8,** 1025–1041.

Fofonoff, N. P., and R. C. Millard Jr., 1983: Algorithms for computation of fundamental properties of seawater. UNESCO Tech. Papers in Marine Science 44, 53 pp. [Available from Division of Marine Sciences, UNESCO, Place de Fontenoy, F-75700, Paris, France. Copy at CNR - Istituto Talassografico di Trieste, viale Romolo Gessi 2, I-34123 Trieste, Italy.]

Franco, P., 1970: Oceanography of Northern Adriatic Sea. 1 Hydrologic features: Cruises July–August and October–November 1965. *Arch. Oceanol. Limnol.,* **XVI**(Suppl. 1), 1–93.

——, 1972: Oceanography of Northern Adriatic Sea. 2 Hydrologic features: Cruises January–February and April–May 1966. *Arch. Oceanol. Limnol.,* **XVII**(Suppl.), 1–97.

——, 1982: Oceanography of Northern Adriatic Sea. Data from the cruises of the years 1978 and 1979. *Arch. Oceanol. Limnol.,* **XX**(Suppl. 2), 33–207.

——, and D. Bregant, 1983: Ingressione invernale di acque dense nord-adriatiche nella fossa del Pomo. *Atti IV Congr. AIOL,* 26/1–26/10.

Gill, A. E., 1982: *Atmosphere–Ocean Dynamics.* International Geophysics Series, Vol. 30, Academic Press, 662 pp.

Grasshoff, K., M. Ehrhardt, and K. Kremling, Eds., 1983: *Methods of Seawater Analysis.* 2d ed. Verlag Chemie, 317 pp.

Hecht, A., Z. Rosentroub, and J. Bishop, 1985: Temporal and spacial variations of heat storage in the Eastern Mediterranean. *Isr. J. Earth Sci.,* **34,** 51–64.

Hellerman, S., and M. Rosenstein, 1983: Normal monthly wind stress over the world ocean with error estimates. *J. Phys. Oceanogr.,* **13,** 1093–1104.

Hendershott, M. C., and P. Rizzoli, 1972: The winter circulation of the Adriatic Sea. *Deep-Sea Res.,* **23,** 353–373.

Hydrographic Institute of the Yugoslav Navy, 1982: Reports and results of the oceanographic investigations in the Adriatic Sea (1974–1976). 239 pp. [Available from CNR - Istituto Talassografico di Trieste, viale Romolo Gessi 2, I-34123 Trieste, Italy.]

Institut za Oceanografiju i Ribarstvo—Split, 1985: Oceanographic data of the cruises made by ships Vila Velebita in 1913 and Hvar in 1948. [Available on magnetic tape from CNR di Istituto Ricerche sulla Pesca Marittima, largo Fiera della Pesca 1, I-60125 Ancona, Italy.]

Jacobsen, J. P., 1921: Dosage de l'oxygen dans l'eau de mer par la méthode de Winkler. *Bull. Inst. Oceanogr. Monaco,* **390,** 3–16.

Kondo, J., 1975: Air–sea bulk transfer coefficients in diabatic conditions. *Bound.-Layer Meteor.,* **9,** 91–112.

Legates, D. R., and C. J. Willmott, 1990: Mean seasonal and spatial variability in gauge-corrected, global precipitation. *Int. J. Climatol.,* **10,** 111–127.

Levitus, S., 1982: *Climatological Atlas of the World Ocean.* NOAA Prof. Paper 13, U.S. Govt. Printing Office, 173 pp. and 17 microfiches.

Malanotte-Rizzoli, P., 1977: Winter oceanographic properties of Northern Adriatic Sea. Cruise January–February 1972. *Arch. Oceanogr. Limnol.,* **19,** 1–45.

May, P. W., 1982: Climatological flux estimates in the Mediterranean Sea: Part I. Wind and wind stresses. NORDA Rep. 54, 56 pp. [Available from Naval Ocean Research and Development Activity, NTSL Station, MS 39529.]

——, 1986: A brief explanation of Mediterranean heat and momentum flux calculations. NORDA Code 322, 1 pp. [Available from Naval Ocean Research and Development Activity, NTSL Station, MS 39529.]

Michelato, A., and V. Kovačević, 1991: Some dynamic features of the flow through the Otranto Strait. *Boll. Oceanol. Teor. Appl.,* **9,** 39–51.

Mosetti, F., and A. Lavenia, 1969: Appendice alla nota: Ricerche Oceanografiche nel Mare Adriatico nel periodo 1966–68. Os-

servatorio Geofisico Sperimentale, Contrib. 189 bis, 1 pp. [Available from Osservatorio Geofisico Sperimentale, P.O. Box 2011, I-34016 Trieste, Italy.]

Orlić, M., M. Gačić, and P. E. La Violette, 1992: The currents and circulation of the Adriatic Sea. *Oceanol. Acta,* **15,** 109–124.

Ovchinnikov, I. M., V. I. Zats, V. G. Krivosheia, and A. I. Udodov, 1985: Formation of deep eastern Mediterranean waters in the Adriatic Sea. *Oceanology,* **25,** 704–707.

Payne, R. E., 1972: Albedo of the sea surface. *J. Atmos. Sci.,* **29,** 959–970.

Pigorini, B., 1968: Aspetti sedimentologici del Mare Adriatico. *Mem. Soc. Ital. Sci. Natl., Museo Civico Storia Natl.,* **16,** 131–199.

Pollak, M. J., 1951: The sources of deep water of the eastern Mediterranean Sea. *J. Mar. Res.,* **10,** 128–152.

R. Comitato Talassografico, 1912: Osservazioni fatte durante le 3 crociere della R. N. Ciclope (I^a–III^a). Commissione Internazionale Permanente per lo studio dell'Adriatico, 54 pp. [Available from CNR—Istituto Talassografico di Trieste, viale Romolo Gessi 2, I-34123 Trieste, Italy.]

——, 1913: Osservazioni fatte durante le crociere della R. N. Ciclope (IV^a–V^a). Commissione Internazionale Permanente per lo studio dell'Adriatico, 41 pp. [Available from CNR - Istituto Talassografico di Trieste, viale Romolo Gessi 2, I-34123 Trieste, Italy.]

——, 1914: Osservazioni fatte durante le 5 crociere della R. N. Ciclope (VI^a–X^a). Commissione Internazionale Permanente per lo studio dell'Adriatico, 93 pp. [Available from CNR - Istituto Talassografico di Trieste, viale Romolo Gessi 2, I-34123 Trieste, Italy.]

Raicich, F., 1994: Note on the flow rates of the Adriatic rivers. CNR, Istituto Talassografico di Trieste Tech. Rep. RF 02/94, 8 pp. [Avaible from CNR–Istituto Talassografico di Trieste, viale Romolo Gessi 2, I-34123 Trieste, Italy.]

Roether, W. and R. Schlitzer, 1991: Eastern Mediterranean deep water renewal on the basis of cholorofluoromethane and tritium data. *Dyn. Atmos. Oceans,* **15,** 333–354.

Rosati, A., and K. Miyakoda, 1988: A general circulation model for upper ocean simulation. *J. Phys. Oceanogr.,* **18,** 1601–1626.

Simpson, J. J., and C. A. Paulson, 1979: Mid-ocean observations of atmosphere radiation. *Quart. J. Roy. Meteor. Soc.,* **105,** 487–502.

Strickland, J. D. H., and T. R. Parsons, 1960: A manual for sea water analysis. *Bull. Fish. Res. Board Can.,* **125,** 1–185.

Stull, R. B., 1988: *An Introduction to Boundary Layer Meteorology.* Kluwer Academic, 666 pp.

Thompson, T. G., and R. J. Robinson, 1939: Notes on the determination of dissolved oxygen in sea water. *J. Mar. Res.,* **2,** 1–8.

Trotti, L., 1969: Crociere Mare Adriatico 1965–1966. Consiglio Nazionale delle Ricerche, Raccolta dati oceanografici, Serie A, No. 29, 82 pp. [Available from CNR–Istituto Talassografico di Trieste, viale Romolo Gessi 2, I-34123 Trieste, Italy.]

U.S. Navy, 1968: Instruction manual for obtaining oceanographic data. U.S. Naval Oceanographic Office Publ. 607, 3d ed., 238 pp. [Available from CNR—Istituto Talassografico di Trieste, viale Romolo Gessi 2, I-34123 Trieste, Italy.]

Vercelli, F., and M. Picotti, 1926: *Il Regime Fisico-Chimico Delle Acque Nello Stretto di Messina.* Commissione Internazionale del Mediterraneo, 163 pp.

Winkler, L. W., 1888: Bestimmung des im Wasser gelösten Sauerstoffes. *Ber. Dtsch. Chem. Ges.,* **21,** 2843–2854.

Zavodnik, D., 1983: 400 years of the Adriatic marine science. *Thalassia Jugosl.,* **19,** 405–429.

Zore-Armanda, M., 1963: Les masses d'eau de la mer Adriatique. *Acta Adriat.,* **10,** 5–88.

——, M. Bone, V. Dadić, M. Morović, D. Ratković, L. Stojanoski, and I. Vukadin, 1991: Hydrographic properties of the Adriatic Sea in the period from 1971 through 1983. *Acta Adriat.,* **32,** 1–544.